

# Physics and optimization of beta-beams: From low to very high gamma

P. HUBER<sup>a</sup>, M. LINDNER<sup>b</sup>, M. ROLINEC<sup>b</sup>, W. WINTER<sup>c</sup>

<sup>a</sup>*Department of Physics, University of Wisconsin,  
1150 University Avenue, Madison, WI 53706, USA*

<sup>b</sup>*Physik-Department, Technische Universität München,  
James-Franck-Strasse, 85748 Garching, Germany*

<sup>c</sup>*School of Natural Sciences, Institute for Advanced Study,  
Einstein Drive, Princeton, NJ 08540, USA*

*September 8, 2018*

## Abstract

The physics potential of beta beams is investigated from low to very high gamma values and it is compared to superbeams and neutrino factories. The gamma factor and the baseline are treated as continuous variables in the optimization of the beta beam, while a fixed mass water Cherenkov detector or a totally active scintillator detector is assumed. We include in our discussion also the gamma dependence of the number of ion decays per year. For low gamma, we find that a beta beam could be a very interesting alternative to a superbeam upgrade, especially if it is operated at the second oscillation maximum to reduce correlations and degeneracies. For high gamma, we find that a beta beam could have a potential similar to a neutrino factory. In all cases, the sensitivity of the beta beams to CP violation is very impressive if similar neutrino and anti-neutrino event rates can be achieved.

---

<sup>a</sup>Email: phuber@physics.wisc.edu

<sup>b</sup>Email: lindner@ph.tum.de

<sup>b</sup>Email: rolinec@ph.tum.de

<sup>c</sup>Email: winter@ias.edu

# 1 Introduction

Future neutrino oscillation experiments with beams will ultimately lead to precise measurements of the leading solar and atmospheric oscillation parameters. This will also lead to precise measurements of  $\sin^2 2\theta_{13}$ , to a determination of the mass hierarchy, and measurements of leptonic CP violation. Long baseline neutrino oscillation experiments constitute therefore a very valuable physics program, since they will provide the most precise information on flavour which will be crucial for progress in our understanding of the origin and the structure of flavour. There exist different experimental paths how precision oscillation measurements can be achieved. Beyond the planned superbeam neutrino oscillation experiments T2K [1] and NO $\nu$ A [2]), one could build upgrades of superbeams (T2HK [3]), neutrino factories [4–6], or  $\beta$ -beams [7–18]. The optimization among these alternatives depends on the outcome of on-going experiments which determine or limit, for example, the actual value of  $\sin^2 2\theta_{13}$ , which determines the CP violation and mass hierarchy measurement reaches. More important are, however, the generic differences between the different options. Since superbeam upgrades are limited by the intrinsic beam background, their performance becomes rapidly suppressed below  $\sin^2 2\theta_{13} \lesssim 10^{-3}$ . Contrary to that, neutrino factories have a clean beam which contains 50% neutrinos and 50% anti-neutrinos of different flavours, which means that they are not limited by an intrinsic beam background. However, neutrino factory detectors must be able to discriminate extremely well between right-sign and wrong-sign muons to discriminate neutrinos and anti-neutrinos [19]. This can be done with magnetized detectors, but it heavily affects the efficiencies especially at low energies, limiting the accessible L/E range. In addition, for a  $\sin^2 2\theta_{13}$  or CP violation search experiment, high event rates turn out to be very important, which means that combinations of high neutrino energies and quite long baselines are favored (see, e.g. [20]).  $\beta$ -beams, on the other side, face neither of these principle disadvantages: They use a pure electron neutrino (anti-neutrino) beam and they can be easily operated at the oscillation maximum at a rather reasonable baseline. Besides there also is a proposal for a very low  $\gamma \sim 10$   $\beta$ -beam which could be used to study neutrino nucleon interactions [21, 22]. Although the insights gained at such a facility would be invaluable to improve our theoretical understanding of neutrino cross sections, we will not discuss this option any further as it would be beyond the scope of this work.

All these novel types of experiments have certainly a number of technological issues which must be further investigated before such facilities can be built. However, the physics questions, such as the optimal  $\gamma$  and baseline combinations for  $\beta$ -beams, should be understood first in order to identify the best options which we should be aiming for.

The answers to such questions depends obviously on the chosen detector technology, external constraints to the setup, and the physical observable for which the optimization of the  $\beta$ -beam is performed. Some of these issues have been previously discussed in detail with a somewhat different focus in [10, 16].

This study addresses the most relevant of these questions. We analyze in detail the optimization of  $\beta$ -beams and we compare the physics potential of  $\beta$ -beams to the one of superbeam upgrades and neutrino factories, where a special emphasis is put on an “equal footing” comparison, *i.e.*, we choose comparable detector sizes and running times.

This study is organized as follows: In chapter 2, we describe the simulation techniques and the parameters used for the beam and for the detectors of this study. The optimization of the  $\sin^2 2\theta_{13}$  sensitivity is then discussed in chapter 3. Special emphasis is here put on the dependence on  $\gamma$ , the baseline and the  $\gamma$  scaling of the number of decays per year. Chapter 4 contains then a discussion of the optimization with respect to the mass hierarchy and CP violation. A summary and conclusions will be given finally in section 5.

## 2 Experiment simulation

In this section, we first describe the properties of the  $\beta$ -beam and the techniques used for the simulation of the experiment. One of the main objectives of this study is to investigate the performance of the  $\beta$ -beam in a wide range of  $\gamma$ . Different choices of  $\gamma$  imply different optimal detector technologies and the description of the detector parameterizations is therefore a key element of this section.

### 2.1 Simulation techniques

All experiment simulations in this study are performed with the GLoBES software [23]. The assumed “true” solar and atmospheric oscillation parameters, which are used as input for the calculation of simulated event rates with GLoBES, are, unless stated otherwise [24–27]:

$$\begin{aligned} \Delta m_{31}^2 &= 2.5 \cdot 10^{-3} \text{ eV}^2, & \sin^2 2\theta_{23} &= 1 \\ \Delta m_{21}^2 &= 8.2 \cdot 10^{-5} \text{ eV}^2, & \sin^2 2\theta_{12} &= 0.83. \end{aligned} \tag{1}$$

The errors of these parameters are given in Refs. [24–27] will also be included in our analysis. For  $\sin^2 2\theta_{13}$ , we only allow values below the CHOOZ bound [28], *i.e.*,  $\sin^2 2\theta_{13} \lesssim 0.1$ . In some cases, we additionally demonstrate the effects for the choice of a smaller true value of  $\Delta m_{31}^2 = 1.5 \cdot 10^{-3} \text{ eV}^2$ , representing the lower end of the currently allowed 90% CL region [27] and, how this affects the performance of the simulated experiments.

The solar oscillation parameters and their errors are included as external input which affect the performance of the discussed setups via correlations. We assume a precision of 5% for  $\Delta m_{21}^2$  and 10% for  $\theta_{12}$ . This corresponds approximately to the current precisions such that this should be a conservative assumption at the time of the discussed experiments [25]. In addition,  $\beta$ -beams cannot determine the leading atmospheric parameters with high precision. Therefore, we combine all of our  $\beta$ -beam simulations, which include effects due to correlations with the atmospheric parameters, with an equivalent of 10 years of T2K running<sup>1</sup>. Data corresponding to this scenario in their combined statistics should be available from T2K, NO $\nu$ A, and atmospheric experiments at the time when a  $\beta$ -beam is analyzed. However, we only use the T2K disappearance channels (and leave out the appearance channels) in order to avoid confusion in the interpretation of  $\beta$ -beam appearance data. This assures that we only include external information on the leading atmospheric parameters. This approach may seem to be more complicated than assuming external precisions for

---

<sup>1</sup>See Refs. [29, 30] for details of the T2K description within GLoBES.

the leading atmospheric parameters. However, if one discusses the effects of parameter degeneracies, it is always a difficult issue *where* (at which point in parameter space) these external precisions for the degenerate solutions should be centered, *i.e.* where the external measurement gives the degenerate solution. Thus, simply assuming external precisions added at some points in parameter space would clearly over-estimate the performance of the  $\beta$ -beams by adding unwanted prior contributions. Including in the analysis an equivalent of 10 years of T2K disappearance running is therefore a simple and quite realistic approach to deal with this problem without creating “artificial” topologies. For the neutrino factory and T2HK simulations, however, it is reasonable to assume that  $\Delta m_{31}^2$  and  $\theta_{23}$  are measured by far best with their own disappearance channels, *i.e.*, we do not impose any external precision on the leading atmospheric parameters there. Eventually, we assume a constant matter density profile with a 5 % uncertainty on the value of the baseline-averaged matter density, where the uncertainty takes into account matter density uncertainties as well as matter density profile effects [31–33]. If the baseline of an experiment is changed, we also re-compute and use the average matter density for this baseline.

## 2.2 Beam characteristics

The neutrino beam discussed in this study is assumed to originate from the beta decay of  ${}^6\text{He}$  and  ${}^{18}\text{Ne}$  isotopes in straight sections of a storage ring. It is assumed that the energy or equivalently the relativistic  $\gamma$  value can be chosen. The corresponding decay channels are:



which leads correspondingly to pure electron neutrino or electron anti-neutrino beams without any intrinsic beam contamination. In the rest frame of the particular decay the neutrinos are emitted isotropically and the energy spectrum is given by the well-known beta decay with a certain endpoint energy for a given isotope. In the storage ring, the spectrum is boosted and it becomes in the laboratory system [10]:

$$\frac{d\phi}{dE_\nu} \propto \frac{E_\nu^2}{\gamma} \left(1 - \frac{E_\nu}{2\gamma(E_0 + m_e)}\right) \sqrt{\left(1 - \frac{E_\nu}{2\gamma(E_0 + m_e)}\right)^2 - \left(\frac{m_e}{E_0 + m_e}\right)^2}. \tag{3}$$

${}^{18}\text{Ne}$  and  ${}^6\text{He}$  are in principle not the only possible choices for the isotopes, but we will use here the same assumption as most of the existing literature [8–13, 15–18]. The endpoint energies  $E_0$  of these two isotopes are very similar. This leads to the nice feature, that they give approximately the same mean neutrino energy at the same  $\gamma$ , *i.e.* we have  $\gamma({}^6\text{He}) = \gamma({}^{18}\text{Ne})$  and there is no obvious gain in increasing one of the two  $\gamma$ ’s (*cf.*, Ref. [16])<sup>2</sup>. The endpoint energies are  $E_0 = 3.4 \text{ MeV}$  for  ${}^{18}\text{Ne}$  and  $E_0 = 3.5 \text{ MeV}$  for  ${}^6\text{He}$ . Note that we neglect the fact that there are different excited states in the daughter nuclei of the decay, which additionally lead to negligible small contributions to the spectra with different endpoint energies.

---

<sup>2</sup>Basically it is fortunate to have a  $\gamma$  as high as possible for each neutrinos and anti-neutrinos independently.

In Ref. [8, 9, 34] it is assumed that  $2.9 \cdot 10^{18}$   ${}^6\text{He}$  and  $1.1 \cdot 10^{18}$   ${}^{18}\text{Ne}$  decays per year can be achieved at a  $\beta$ -beam scenario with the acceleration  $\gamma({}^{18}\text{Ne}) = 100$  and  $\gamma({}^6\text{Ne}) = 60$  at the same time. If not stated differently, we assume that the number of decays per year stays constant with varying  $\gamma$ . However, since this assumption is most likely not justified from technological considerations, we also describe effects where the number of decays varies with  $\gamma$  with the above values as normalization at  $\gamma({}^{18}\text{Ne}) = 100$  and  $\gamma({}^6\text{Ne}) = 60$ .

For all discussed  $\beta$ -beam setups, we choose a total running time of 8 years. This implies that the number of ion decays above are assumed to be reached by either the simultaneous operation of the neutrino and anti-neutrino beams, or their **double** numbers by the successive operation of four years neutrinos and four years anti-neutrinos. We will also discuss deviations from equal neutrino and anti-neutrino running which could be achieved by successive operation option or by changing the ratio of stored ions. However, as default we use equal running times for neutrinos and anti-neutrinos, since the performance for quantities highly correlated with  $\delta_{\text{CP}}$  is usually best for equal statistics in the neutrino and anti-neutrino channels, and the higher anti-neutrino flux turns out to compensate for the lower anti-neutrino cross section very well.

## 2.3 Detector technologies

A general requirement for any  $\beta$ -beam detector is to have good muon-electron separation capabilities and to have an efficient neutral current rejection. At the same time, the technology must be available and cost effective to allow in time a scaling to large detectors. For lower values of  $\gamma$ , certainly Water Cherenkov detectors (WC) fulfill these criteria [7, 9, 10, 12, 15, 16]. However, at higher  $\gamma$  values, the lack of background discrimination in WCs becomes a huge problem and other detector types, such as calorimeters or TPCs (Time Projection Chambers) are more suitable [10, 35]. The precise value of  $\gamma$  where this turnover happens seems to be an unresolved question and quite different views can be found in the literature [9, 10]. We will describe our own approach to this problem and we will discuss our findings in relationship to the existing literature. Our choice for large values of  $\gamma$  is the so called “Totally Active Scintillator Detector” (TASD) for reasons which will be discussed below. The two detector technologies used in this study, namely WC and TASD, are described in more detail in the following subsections.

### 2.3.1 Water Cherenkov detector

Water Cherenkov detectors are well suited to distinguish muon neutrinos from electron neutrinos. However, background rejection can be a problem in using a WC detector in combination with a  $\beta$ -beam. The main source of background to the muon neutrino appearance search will be the flavour-blind neutral current events which are mistaken for muon neutrino charged current events. The most critical neutral current events are those where one or several energetic pions are involved, which implies that there is basically no background below the pion production threshold around 200 MeV. Therefore, one solution would be to tune  $\gamma$  to a low value where most of the neutrinos in the beam are below this threshold [9]. In that case there would be no energy information, since the Fermi-motion of the nucleons

	Case A		Case B		This work	
	$\nu$	$\bar{\nu}$	$\nu$	$\bar{\nu}$	$\nu$	$\bar{\nu}$
Signal	3128	3326	2956	3261	3129	3313
Background	514	588	176	123	170	123

**Table 1:** The total signal and background rates in a Water Cherenkov detector at  $L = 300$  km for an overall exposure of 5000 kty with a  $\beta$ -beam at  $\gamma = 150$  for neutrinos and anti-neutrinos. The oscillations parameters are the ones from Eq. (1) and  $\sin^2 2\theta_{13} = 0.1$ . “case A” corresponds to Ref. [9, 36, 37] and “case B” to Ref. [16].

would induce an energy smearing of about 100 MeV. This would reduce the  $\beta$ -beam to a mere counting experiment, which would have only a very limited physics reach [10]. Above the pion threshold, the feasibility of using a WC detector depends on the ability to correctly identify pions and to reject neutral current events. The pion identification works, in principle, by identifying its decay process and it seems to be possible up to some level. There are very different statements in the literature how well this can be done [9, 10]. The different results can to a large extent be attributed to the different level of detail used in the detector simulation. Nonetheless we will show a direct comparison of the two simulations and our parameterization at a reference scenario with  $\gamma = 150$  at a baseline of  $L = 300$  km and an overall exposure equivalent to 5000 kty, where we call the one from Ref. [9, 36, 37] “case A” and the one from Ref. [16] “case B”. As one can see from Table 1, the number of signal events is very similar in both cases, but the number of background events is very different. Moreover, the shape of the background spectra is very different and the background events are much more concentrated at low energies for case B.

The simulation of case B is based on the Super-Kamiokande Monte-Carlo [38] and it seems to be more detailed in its treatment of detector effects. For this reason we use a parameterization which is, in total rates very close to case B, as can also be seen from Table 1. Note, however, that even though the Monte-Carlo used for case B has been well-tested in Super-Kamiokande, it is important to keep in mind that such simulations rely on physical input such as cross sections, which are not very well known. Moreover, the assumption that the response of a 20 times larger detector is the same as that of Super-Kamiokande is implied there.

In order to describe the energy response of the detector in our study, we divide the signal events into samples of quasi-elastic events (QE) and inelastic events (IE). Only for the QE sample, it is possible to accurately reconstruct the neutrino energy from the charged lepton. For IE events, the reconstructed energy will always lie below the true (incident) neutrino energy because the hadronic component of the interaction cannot be seen by a WC detector. Since the separation of those two event samples is fraught with a large error, we will use the same technique as described in Ref. [29]. This means that the total rates number of all IE + QE events is taken and in addition the spectrum of the QE event sample is used to obtain spectral information. In order to avoid double counting of events, the QE event sample is taken only with a free normalization. In this approach, no particular assumption about the event by event separation has to be made, because this approach is purely statistical.

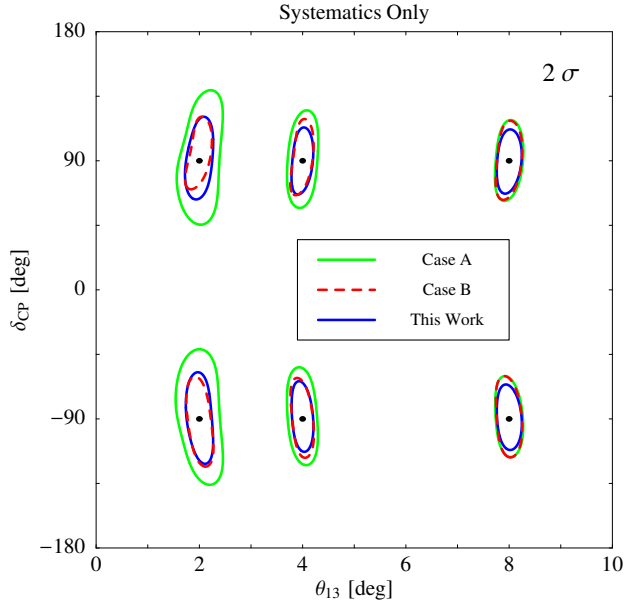


**Figure 1:** The allowed regions in the  $\theta_{13}$ - $\delta_{\text{CP}}$ -plane at  $2\sigma$  CL with only systematics taken into account. The solid green (bright gray) curve corresponds to case A, the dashed red (dark gray) curve to case B, and the solid blue (black) curve to the scenario used in this study. The black dots indicate the values of  $\theta_{13}$  and  $\delta$  used as input (true values) and the other oscillation parameters are the ones from Eq. (1).

In fact, the real experiment might even perform better since there actually could be some event by event separation. For the spectral analysis, we assume that the Fermi-motion is the main component of the resulting energy resolution function. Therefore, a constant width of 85 MeV [1] in a Gaussian energy resolution function is taken, in order to describe the energy reconstruction of the QE sample. For the background distribution, we make the assumption that every neutrino which interacts via neutral currents is reconstructed with an energy distribution which is flat from zero up to the true neutrino energy. In this way we obtain a background which is peaked at low energies very similar to the one in case B. We do not take into account any other background source, since in Ref. [16] it was shown that atmospheric neutrinos only give a very small contribution.

Figure 1 shows a comparison of the physics output of the cases A, B and our parameterization. The allowed regions in the  $\theta_{13}$ - $\delta$  plane at a confidence level of  $2\sigma$  for 2 d.o.f. are shown assuming that all the other parameters are exactly known and have the values as in Eq. (1). Case B (dark gray/red curves) and our parameterization (black/blue curves) agree very well throughout the parameter space. The numbers used for our parameterization can be found in Table 2.

In order to be able to use  $\gamma$  values in the range from 50 to 500, the energy range is chosen as 0.2 – 3.0 GeV and is divided into bins of 100 MeV width, such that the total number of bins is 28. All efficiencies are constant with exception of the first bin where they are only 1/2 of the value given in Table 2 to account for threshold effects. The numbers for the disappearance channel could be quite different (in fact, the efficiencies might be much

	Appearance		Disappearance	
	$\nu$	$\bar{\nu}$	$\nu$	$\bar{\nu}$
Signal efficiency	0.55	0.75	0.55	0.75
Background rejection	0.003	0.0025	0.003	0.0025
Signal error	2.5%	2.5%	2.5%	2.5%
Background error	5%	5%	5%	5%

**Table 2:** The signal efficiencies and background rejection respectively and the systematical errors for the various signals and backgrounds used in our description of the performance of a Water Cherenkov (WC) detector.

higher), but we checked that the final results do not depend on this assumption. Therefore, because of simplicity, we take the same numbers as for the appearance channels. We also include systematic uncertainties on the normalization of signal and background events as given in Table 2, where all errors are assumed to be fully uncorrelated. This is a conservative approximation and does not affect the result from the appearance measurement. The disappearance measurement, on the other hand, would require a total absolute error of less than 1% to yield any information on  $\theta_{13}$  [39–41]. This number, however, seems very difficult to be reached, if at all, for any experiment which involves neutrino-nucleus cross-sections at low energies. Our parameterization has been calibrated against case B for  $\gamma = 150$ . Therefore using different values of  $\gamma$  involves some extrapolation. Our parameterization should nevertheless be reliable from  $\gamma = 100$  up to 350, and it should additionally reproduce the qualitative features of the  $\gamma$ -scaling within a range from 50 to 500.

### 2.3.2 Totally active scintillator detector

For even larger values of  $\gamma$ , a detector which can also measure the hadronic energy deposition is required. The reason is that the fraction of inelastic events in the whole event sample increases with increasing  $\gamma$ , because the neutrino spectra are extended to higher energies. The techniques which have traditionally been used for that purpose are tracking calorimeters and TPCs (such as a large liquid Argon TPC as described in Ref. [35]). The latter technology has certainly a great potential in neutrino physics, but given the fact that background issues are not the primary concern, we will discuss the more traditional and better understood option of a tracking calorimeter. Basically, there exist three different approaches:

- magnetized iron plates, interleaved with scintillator bars
- low-Z material (such as particle board), interleaved with scintillator bars
- all active detector made of liquid scintillator and plastic tubes

The big advantage of a (magnetized) iron calorimeter is usually the ability to determine the charge of muons, but this is pointless for a  $\beta$ -beam since there is no appearance of wrong

	Appearance		Disappearance	
	$\nu$	$\bar{\nu}$	$\nu$	$\bar{\nu}$
Signal efficiency	0.8	0.8	0.2	0.2
Background rejection	0.001	0.001	0.001	0.001
Signal error	2.5%	2.5%	2.5%	2.5%
Background error	5%	5%	5%	5%

**Table 3:** The signal efficiencies and background rejection respectively and the systematical errors for the various signals and backgrounds used in our description of a TASD.

sign muons like at a neutrino factory. For the other options, the advantages and disadvantages have been very carefully addressed in the preparation of the NO $\nu$ A proposal [2]. We decided to use for our study the same technology as in the NO $\nu$ A proposal, which is the so called “Totally Active Scintillator Detector” (TASD). The totally active design provides a superior energy resolution and background rejection at reasonable efficiencies. For our parameterization, we follow closely the work done by the NO $\nu$ A collaboration, the only problem being that all studies have been done for  $\nu_e$  appearance, whereas we look for  $\nu_\mu$  appearance. The latter should be much easier because the muon track is much more difficult to be confused with a neutral current event. Therefore, our parameterization is on the conservative side, which does not affect our conclusions since the TASD very effectively rejects backgrounds. The numbers we use for efficiencies and systematical errors are given in Table 3 and are taken from Refs. [2, 42–44].

The energy window reaches from 0.5 GeV up to the endpoint of the neutrino spectrum and is divided into 20 bins. The energy resolution is given by a Gaussian with a width of 3%  $\sqrt{E}$  for muon neutrinos and 6%  $\sqrt{E}$  for electron neutrinos. The background is assumed to have the same shape as the signal. But note that the shape of the background is not much of an issue in the case of a TASD detector since the background is very small. We checked that a background of the same total magnitude which is distributed like  $E_\nu^{-1}$  gives basically the same results.

## 2.4 Experiment configurations and event rates

In order to compare the different detector options we still need to define the detector size and the luminosity of the beam. The fiducial volume of a WC detector seems to lie naturally of the order of 1 Mt, since this suits also other applications as proton decay searches and there exists various proposals of this type, see *e.g.* Ref. [45]. For definiteness, we assume our WC detector of this type, but with a somewhat more affordable fiducial volume of 500 kt. For the TASD there exists currently only the NO $\nu$ A proposal for a 30 kt detector, and 50 kt’s seem to be feasible. We will use therefore the latter (larger) value as the detector mass of the TASD within this study. Within the usual uncertainties, these two detectors should also have a comparable price. These two choices lead to the typical signal and background event rates shown in Table 4 for the true parameters of Eq. (1) and  $\sin^2 2\theta_{13} = 0.1$ . Note, however, that these numbers are calculated under the assumption of a constant number of isotope decays. This will of course change when we include the  $\gamma$ -scaling in subsequent

Detector type	WC	TASD	TASD
$m$ [kt]	500	50	50
$\gamma$	200	500	1000
$L$ [km]	520	650	1000
$\nu$ signal	1983	2807	7416
$\nu$ background	105	31	95

**Table 4:** The number of signal/background events for different combinations of the chosen detector type and values of  $\gamma$ . These numbers are calculated for constant number of isotope decays per year with varying  $\gamma$ . The oscillation parameters are the same as in Eq. (1) with  $\sin^2 2\theta_{13} = 0.1$ .

sections.

### 3 Optimization of $\sin^2 2\theta_{13}$ sensitivity

In this section, we focus on the optimization of detecting a finite value and/or measuring  $\sin^2 2\theta_{13}$ . For that, we introduce performance indicators for the sensitivity to  $\sin^2 2\theta_{13}$  and discuss the principle degrees of freedom for the optimization. Furthermore, we illustrate the optimization in the most relevant directions of the parameter space and choose specific setups. Eventually, we compare the performance to other established techniques, such as neutrino factories or superbeam upgrades.

#### 3.1 Degrees of freedom and performance indicators

The optimization of a  $\beta$ -beam experiment involves a number of issues:

- What is the optimal  $\gamma$ ? Obviously, the detector technology is a major issue in this optimization. In addition, external constraints may cause the number of decays per year not to stay constant with increasing  $\gamma$ .
- What is the optimal baseline for a given  $\gamma$ ?
- How long should one run in the  $\nu$  and  $\bar{\nu}$  running mode? At the same or different  $\gamma$ 's? Can one run these modes simultaneously?
- What isotopes should one use? How many decays per year are realistic?

We will discuss some of these issues in greater detail below, while we will make reasonable assumptions in other cases. Let us first repeat the main assumptions which have already been discussed: We assume neutrino and anti-neutrino beams from the decay of  ${}^6\text{He}$  and  ${}^{18}\text{Ne}$  isotopes with the reference numbers for the decays per year at  $\gamma({}^6\text{He}) = 60$  and  $\gamma({}^{18}\text{Ne}) = 100$  as in Ref. [8, 9, 34]. In general, we assume a successive operation with neutrinos and anti-neutrino running, since we will allow a variation of the neutrino versus antineutrino running time in some cases. Furthermore, we fix  $\gamma({}^6\text{He}) = \gamma({}^{18}\text{Ne})$ , since there

is no obvious gain in increasing one of the two  $\gamma$ 's (*cf.*, Ref. [16]). We also use a constant,  $\gamma$  independent detector mass for an assumed Water Cherenkov (WC) or a Totally Active Scintillator Detector (TASD). The WC detector will be used only below  $\gamma \sim 500$ , since for higher energies the WC detector will be dominated by non-QE events and the background parameterization is rather unclear.

Somewhat more complicated is the issue of the  $\gamma$ -dependence of the beam. Initially we will assume that the number of decays per year does not depend on  $\gamma$ , but this is definitively not realistic. We will therefore discuss in detail the impact of a scaling with  $\gamma$  later.

We use two different performance indicators for  $\sin^2 2\theta_{13}$ . We define the  $\sin^2 2\theta_{13}$  sensitivity as the largest value of  $\sin^2 2\theta_{13}$  which fits  $\sin^2 2\theta_{13} = 0$ , *i.e.*, the  $\sin^2 2\theta_{13}$  sensitivity tests the hypothesis  $\sin^2 2\theta_{13} = 0$ . It corresponds to the new exclusion limit if an experiment does not observe a signal. Since the simulated rate vector is computed for  $\sin^2 2\theta_{13} = 0$ , this sensitivity does not depend on the true (simulated) values of  $\sin^2 2\theta_{13}$ ,  $\delta_{\text{CP}}$ , or the mass hierarchy (*cf.*, Appendix C of Ref. [46]). However, there are strong correlations and degeneracies in the fit rate vector because any combination of parameters which fits  $\sin^2 2\theta_{13} = 0$  destroys the  $\sin^2 2\theta_{13}$  sensitivity. In particular, we compute the statistics and systematics  $\sin^2 2\theta_{13}$  sensitivity for fixed  $\delta_{\text{CP}} = 0$  and the other oscillation parameters fixed to their simulated values. The correlation with  $\delta_{\text{CP}}$  and the other oscillation parameters will then be included by the projection of the fit manifold onto the  $\sin^2 2\theta_{13}$ -axis as the correlation bar of our figures, where only the best-fit solution is used. Any disconnected solution at the chosen confidence level which fits  $\sin^2 2\theta_{13} = 0$  is treated as degeneracy, such as a  $(\delta_{\text{CP}}, \theta_{13})$  [47] or mass hierarchy [48] degeneracy. Thus, we treat connected degenerate solutions (with the best-fit manifold) as correlations, and disconnected degenerate solutions as degeneracies.

In addition to the  $\sin^2 2\theta_{13}$  sensitivity, we show the  $\sin^2 2\theta_{13}$  discovery reach in some cases, which tests the hypothesis of observing a signal for a given set of true values. Thus, the  $\sin^2 2\theta_{13}$  discovery reach strongly depends on the true values of  $\sin^2 2\theta_{13}$ ,  $\delta_{\text{CP}}$ , and the mass hierarchy. However, there are almost no correlations or degeneracies, since the fit rate vector is computed for  $\sin^2 2\theta_{13} = 0$ . In principle, the risk-minimized (with respect to the possible true values)  $\sin^2 2\theta_{13}$  discovery reach is comparable to the  $\sin^2 2\theta_{13}$  sensitivity – though the problem is not exactly symmetric.

### 3.2 Performance as function of $\gamma$ and baseline optimization

A first important optimization question concerns the optimal value of  $\gamma$ . Naively this question seems to be trivial for a fixed number of decays per year - the higher the  $\gamma$ , the better. However, there is a strong dependence on detector technology, since non-QE events will start to dominate a WC detector for higher energies, and the efficiency of a TASD (or iron calorimeter) is very low at low energies because of too short tracks compared to the positional information of the detector. We show therefore in Figure 2 the  $\sin^2 2\theta_{13}$  sensitivity for the WC detector (left) and the TASD (right) as function of  $\gamma$ , where the parameterization of the WC detector is most reliable in the unshaded region. For the  $L/\gamma$ , we assume 1.3 for both detectors. Note, however, that we will find that  $L/\gamma = 1.3$  is not optimal for the Water Cherenkov detector if one includes correlations and degeneracies. For the TASD, the rule “the higher the  $\gamma$ , the better” obviously applies if the stored ion

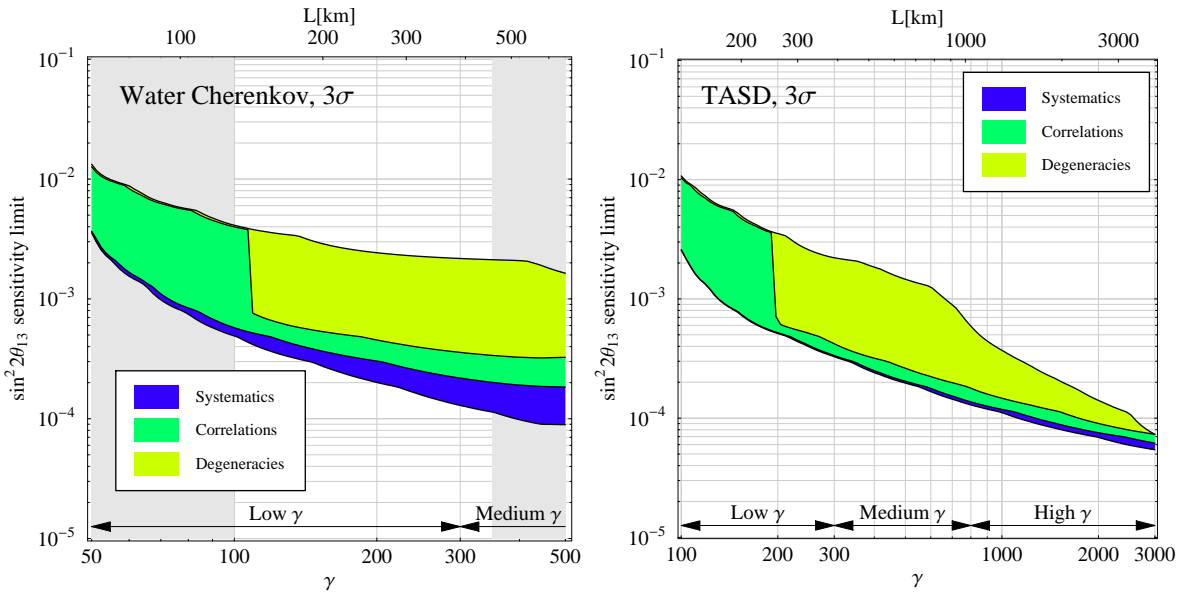


**Figure 2:** The  $\sin^2 2\theta_{13}$  sensitivity limit as function of  $\gamma$  for a constant number of decays per year (as function of  $\gamma$ ) and  $L = 1.3\gamma$  at the  $3\sigma$  confidence level. The plots are for the Water Cherenkov detector (WC, left) and Totally Active Scintillator Detector (TASD, right). The final sensitivity limits are obtained as the upper edges of the curves after successively switching on systematics, correlations, and degeneracies.

decays are constant in  $\gamma$ , since the muon tracks are in average fully contained in the shown range. For the WC detector, this rule also applies in the unshaded region, but it is likely that background domination and non-QE events will affect the performance for higher  $\gamma$ . In addition, the dependence on  $\gamma$  is much more shallow in the considered range, and the impact of systematics increases with increasing  $\gamma$ . Note that though the Water Cherenkov detector has the better systematics only performance at the upper end of the unshaded region (left panel), both detectors perform very similar after including correlations and degeneracies in this range.

The baseline dependence of the  $\sin^2 2\theta_{13}$  sensitivity on  $L/\gamma$  is shown in Figure 3 for different choices of (fixed)  $\gamma$  as given in the plot labels. The optimal  $\sin^2 2\theta_{13}$  sensitivity can in all cases be achieved from a statistical and systematical point of view for  $L/\gamma \sim 0.8 - 1.3$ , where the appearance events only come from the first oscillation maximum. For higher values of  $L/\gamma$  the statistics  $\sin^2 2\theta_{13}$  sensitivity decreases due to the  $1/L^2$  dependence of the flux although the actual position of the first oscillation maximum, taking into account the average neutrino energy, would be at  $L/\gamma \sim 2.1$ . However, longer baselines, where appearance events from the second oscillation maximum enter the energy window of the analysis, have altogether a better potential to resolve correlations and degeneracies. The combined effect of the first and second oscillation maximum together leads to a better determination of the oscillation pattern and larger matter effects, though the statistic limit becomes worse. For the WC detector, we therefore choose  $L/\gamma = 2.6$ , where the impact of correlations and degeneracies is marginal and the overall performance is significantly improved. We demonstrate in Appendix A in detail where this better performance comes from and why it

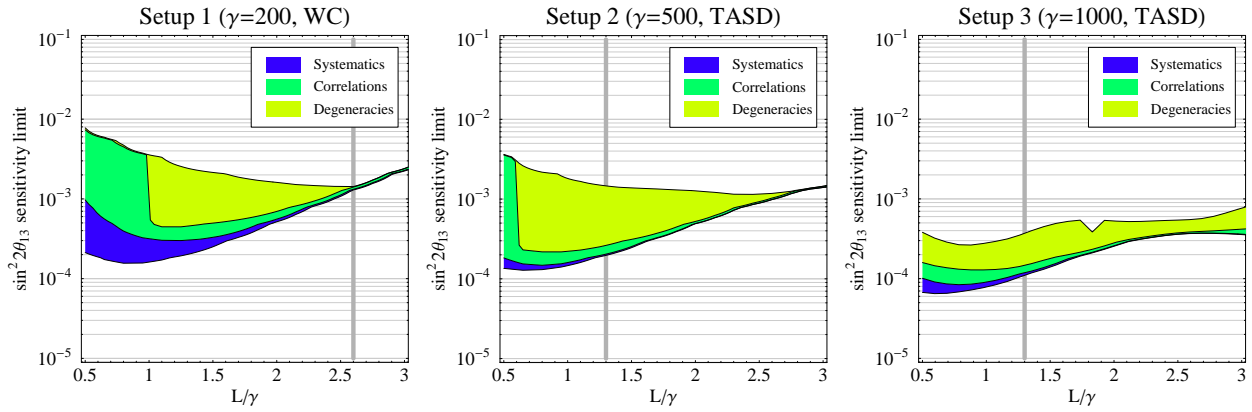


**Figure 3:** The  $\sin^2 2\theta_{13}$  sensitivity limits at the  $3\sigma$  confidence level for the different setups as function of the ratio  $L/\gamma$  for the number of decays per year fixed. Note that  $\gamma$  in each individual plot is fixed to the value given in the respective figure caption. The final sensitivity limits are obtained as the upper edges of the curves after successively switching on systematics, correlations, and degeneracies.

is only visible after the inclusion of correlations and degeneracies. Furthermore, we choose  $L/\gamma = 1.3$  for the TASD, since a larger  $L/\gamma$  hardly improves the performance. In addition, we have tested that if the number of decays per year significantly drops with increasing  $\gamma$ , the minimum of Setup 3 is shifted towards longer baselines. Note that in all cases the flatness in  $L/\gamma$  implies that the precise baseline is not so important for the overall  $\sin^2 2\theta_{13}$  sensitivity. In addition, the choice of these values for  $L/\gamma$  cannot be entirely based upon this figure and will be later justified in the context of different performance indicators.

Let us now directly compare the two detector technologies in Figure 4, where the gray curves correspond to the WC detector and the black curves to the TASD. For small  $\gamma$ , the WC detector obviously has the best performance, whereas for higher  $\gamma$ , the TASD is the way to go for. The crossing point between the two technologies depends on the confidence level and lies somewhere in the interval  $250 \lesssim \gamma \lesssim 500$ . Note, however, that the TASD performance is dominated by correlations and degeneracies (*cf.*, Figure 2), which means that its discovery potential will certainly be better for  $\gamma = 500$  at all confidence levels. In addition, the parameterization of the WC detector is not very reliable in this region anymore.

In order to discuss some effects in greater detail we use well defined setups/representatives in order to evaluate the requirements for a  $\beta$ -beam. Comparing with Figure 4, there are three interesting (approximate) ranges:

1. Low  $\gamma \lesssim 300$ : This range can be probed with relatively “small” accelerators, such as of SPS size, and WC detectors. The physics potential could compete with superbeam upgrades, such as an upgrade of T2K to a Hyperkamiokande detector, or an intermediate step towards a neutrino factory.
2. Medium  $300 \lesssim \gamma \lesssim 800$ : In this case, larger accelerator rings are required, for example of Tevatron size. The detector technology could be WC or TASD. The physics goal could be to compete with superbeam upgrades or even small neutrino factories.

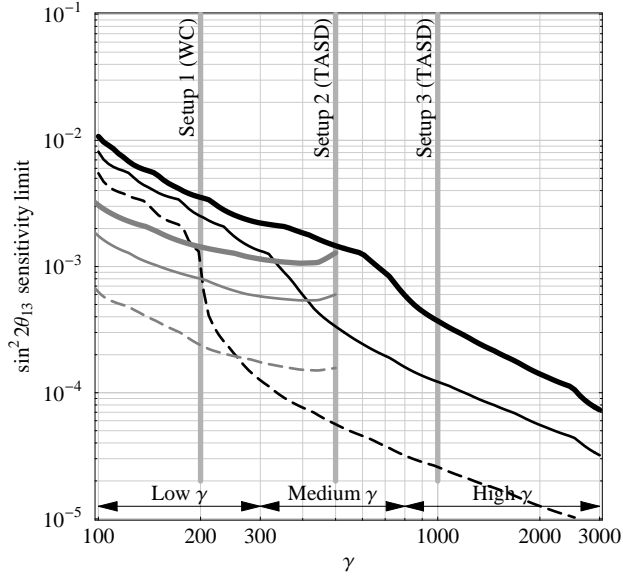


**Figure 4:** The final  $\sin^2 2\theta_{13}$  sensitivity limit (including systematics, correlations, and degeneracies) as function of  $\gamma$  for a fixed number of decays per year. The curves correspond to the Totally Active Scintillator Detector ( $L = 1.3\gamma$ , TASD, black curves) and the Water Cherenkov detector ( $L = 2.6\gamma$ , WC, gray curves) at the  $1\sigma$  (dashed),  $2\sigma$  (thin solid), and  $3\sigma$  (thick solid) confidence levels. The vertical lines correspond to our low-, medium-, and high- $\gamma$  setups. Note that the WC parameterization is only reliable for  $100 \lesssim \gamma \lesssim 350$ .

3. Large  $\gamma \gtrsim 800$ : Very large accelerators of the size of the LHC are required<sup>3</sup>. TASD or iron calorimeters are possible choices for the detector technologies. In this case, the goal is clearly competition with neutrino factories for all of the relevant measurements.

These  $\gamma$ -ranges are shown in many figures of this and the next chapter. Obviously, the requirements for all of these ranges are somewhat different, which means that it will not only be sufficient to compare  $\beta$ -beam with  $\beta$ -beam, but it will also be necessary to compare individual  $\beta$ -beams from each range with its competitors. For this purpose, we define three setups from these three ranges (*cf.*, Figure 4):

- **Setup 1 ( $\gamma = 200$ , WC):** In this case, the WC detector representation is well-established and  $\gamma$  should not be too high for SPL-sized accelerators.
- **Setup 2 ( $\gamma = 500$ , TASD):** This setup represents the lowest  $\gamma$  where a TASD will likely perform better than a WC detector at all confidence levels.
- **Setup 3 ( $\gamma = 1000$ , TASD):** This representative corresponds to a very sophisticated option close the upper limit of what is doable.

---

<sup>3</sup>Note, however, that even though the LHC would have enough energy, it certainly does not have enough RF acceleration power, *i.e.*, a new huge accelerator would be required in this case.

### 3.3 Isotope decay scaling

We have already mentioned that the number of decays per year is most likely not constant in  $\gamma$ . In order to include this effect, we use the following power law parameterization, which should be justified for a certain  $\gamma$ -range, to describe this scaling with  $\gamma$  ( $i = 1$  for  $^{18}\text{Ne}$ : neutrinos,  $i = 2$  for  $^6\text{He}$ : anti-neutrinos>):

$$N^i = N_0^i \cdot \left( \frac{\gamma_0^i}{\gamma} \right)^n \quad (4)$$

Here  $N_0^i$  is determined by our reference point at  $\gamma_0^1 = 100$ ,  $\gamma_0^2 = 60$ . We can now discuss different cases for  $n$ , which leads to different optimization strategies:

- $n = 0$ : The number of decays per year is fixed. This implies that the accelerator and storage ring has to scale appropriately with  $\gamma$  in a non-trivial manner.
- $0 < n < 1$ : This seems to be the most likely range of realistic cases. The number of decays per year becomes constrained with increasing  $\gamma$  by the geometry of the accelerator and decay ring and  $\gamma$  increased lifetime of the isotopes in the laboratory system.
- $n \sim 1$ : This case corresponds to a fixed setup constraining the performance. Given the scaling of the baseline, the number of events stays approximately constant as function of  $\gamma$ . A realistic constraint for the SPS would be, for example,  $n \sim 1$  from the number of merges in the decay ring and the number of ions per bunch [49].
- $n > 1$ : In this case, it clearly does not make sense to go to higher  $\gamma$ 's, since the event rate decreases with  $\gamma$  if we stay in the oscillation maximum
- $n < 0$ : The number of decays per year increases with  $\gamma$ . This hypothetical (but technologically unlikely) possibility requires that the accelerator and decay ring over-proportionally scale with  $\gamma$ .

We further on consider the range  $0 \lesssim n \lesssim 1$  to be realistic. However, it is conceivable that, for a given setup, the performance will scale with  $n \simeq 0$  in the beginning, and change into an  $n \simeq 1$  scaling in the saturation regime.

We show in Figure 5 the  $\gamma$ -scaling of the final  $\sin^2 2\theta_{13}$  sensitivity (including correlations and degeneracies) for the different detector technologies and  $0 \lesssim n \lesssim 1$  (bands), where the solid lines correspond to  $n = 0.5$ . For  $n \sim 1$  (upper ends of bands), the performance is rather flat in  $\gamma$ . This simply means that the increase in cross section is compensated by the  $\gamma$ -scaling. For  $n \sim 0$  (lower end of bands), the  $\sin^2 2\theta_{13}$  sensitivity scales as discussed above. It is interesting to observe that Setups 1 and 2 are much less affected by a decreasing number of decays than Setup 3, which over-proportionally loses sensitivity for  $n > 0$ . Thus, for Setup 3, it is crucial that the accelerator and storage design allow enough decays per year, whereas for Setups 1 and 2 a certain loss in the number of decays results only in about a factor of two weaker sensitivity limit. This means that, given a specific accelerator (such as the LHC), it makes only sense to discuss very high  $\gamma$  setups if it is guaranteed that enough

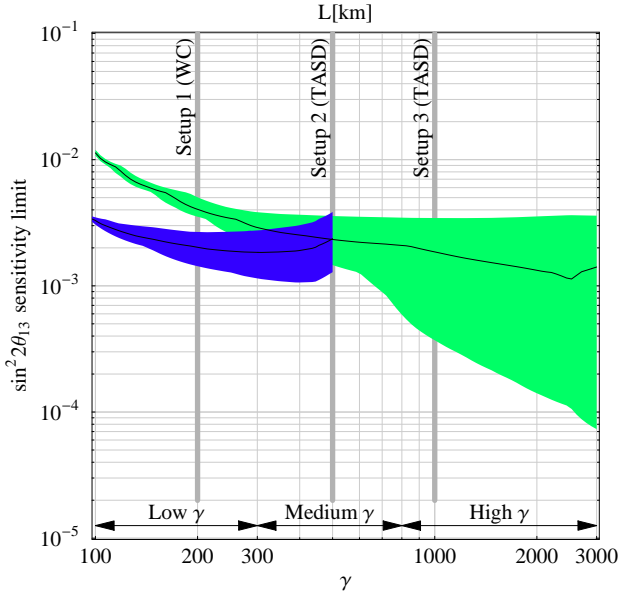


**Figure 5:** The final  $\sin^2 2\theta_{13}$  sensitivity limit (including systematics, correlations, and degeneracies) as function of  $\gamma$  for  $L = 1.3\gamma$  (TASD) and  $L = 2.6\gamma$  (WC). The bands correspond to the Totally Active Scintillator Detector (TASD, green/light shaded region) and the Water Cherenkov detector (WC, blue/dark shaded region) at the  $3\sigma$  confidence level, where the isotope luminosity exponent  $n$  is varied from 0 (lower ends of the bands) over 0.5 (black curves) to 1 (upper end of the bands). The vertical lines correspond to our low-, medium-, and high- $\gamma$  setups.

ions can be stored. Note that the dependence on  $n$  is therefore an important constraints for the  $\gamma$  optimization of  $\beta$ -beams, since, for the TASD, it constrains the rule “the larger  $\gamma$ , the better”.

### 3.4 Comparison with other technologies

Next we compare the  $\sin^2 2\theta_{13}$  sensitivity of  $\beta$ -beams to neutrino factories and superbeam upgrades. For the neutrino factory, we use the representative NuFact-II from Ref. [29] which uses only  $\nu_\mu$  appearance and disappearance in two different baseline configurations  $L = 3\,000\text{ km}$  and  $L = 7\,500\text{ km}$  (NF@3000km and NF@7500km). This assumes 4 MW target power (corresponding to about  $1.06 \cdot 10^{21}$  useful muon decays per year), a 50 kt fiducial volume magnetized iron calorimeter, and 50 GeV neutrinos. The longer baseline corresponds to the “magic baseline”, where correlations and degeneracies are resolved, but no  $\delta_{\text{CP}}$  measurement is possible [50]. The  $\sin^2 2\theta_{13}$  sensitivity and mass hierarchy sensitivity of the neutrino factory at the magic baseline is therefore very competitive. We include this option because we want to compare optimized setups (for particular purposes) with optimized setups later, *i.e.*, the optimal  $\beta$ -beam for the mass hierarchy measurement may also have a different baseline than the one for the CP violation measurement. For the superbeam upgrade, we choose T2HK from Refs. [1] simulated in Ref. [29], but we reduce the fiducial mass to 500 kt and use the same detector as in this study in order to be comparable

Label	$\gamma$	L/km	$\langle E_\nu \rangle$ /GeV	Detector	$m_{\text{Det}}/\text{kt}$	$t_{\text{run}}/\text{yr}$	Ref. ( $\nu, \bar{\nu}$ )
Setup 1	200	520	0.75	Water Cherenkov	500	(4,4)	
Setup 2	500	650	1.9	TASD	50	(4,4)	
Setup 3	1000	1300	3.8	TASD	50	(4,4)	
T2HK*	n/a	295	0.76	Water Cherenkov	500	(2,6)	[29]
NF@3000km	n/a	3000	33	Magn. iron calor.	50	(4,4)	[29]
NF@7500km	n/a	7500	33	Magn. iron calor.	50	(4,4)	[50]

**Table 5:** The experiment representatives used in this study, where all detector masses are fiducial masses. Note that we adjusted the detector mass of T2HK\* compared to Ref. [29] and use the identical detector to Setup 1.

to our WC detector for Setup 1. This superbeam upgrade also assumes a target power of 4 MW and we call it therefore T2HK\*. The different setups are summarized in Table 5.

Figure 6 shows the  $\sin^2 2\theta_{13}$  sensitivity for these setups. First, it is interesting to observe that all of the  $\beta$ -beam representatives are competitive to the T2HK\* setup in all cases. The neutrino factory at  $L = 3000$  km can, for the chosen parameter values, not resolve the  $(\delta, \theta_{13})$ -degeneracy at the  $3\sigma$  confidence level<sup>4</sup>, and therefore the final  $\sin^2 2\theta_{13}$  sensitivity is much worse than that of the  $\beta$ -beams. The neutrino factory at  $L = 7500$  km has the best overall performance because it is hardly affected by the correlation with  $\delta_{\text{CP}}$ . Note that Setup 1 has a better final  $\sin^2 2\theta_{13}$ -sensitivity than Setup 2 because of the choice of  $L/\gamma = 2.6$ . Though the statistics limit is worse for this choice, the correlation and degeneracy bars become very small and lead to a better final sensitivity than for  $L/\gamma = 1.3$ .

In order to complete the picture, we show in Figure 7 the  $\sin^2 2\theta_{13}$  discovery reach as function of the true values of  $\sin^2 2\theta_{13}$ ,  $\delta_{\text{CP}}$  (stacked to the “CP fraction”), and the mass hierarchy. Though the  $\sin^2 2\theta_{13}$  sensitivity of Setup 1 is slightly better than one of Setup 2, one can clearly see that there is a hierarchy in the discovery reach: The choice of Setups 1, 2 and 3 implies that their differences correspond to approximately equal improvements in terms of fraction of the parameter space. The large impact of correlations on the  $\sin^2 2\theta_{13}$  sensitivity of Setup 2 (cf., Figure 6), which mainly comes from the correlation with  $\delta_{\text{CP}}$ , implies that the discovery reach is in many cases of  $\delta_{\text{CP}}$  better than the one of Setup 1. Note that the relative position of the Setup 1 curve would not significantly change with a different choice of  $L/\gamma = 1.3$  because in this case the shape of the curves would be very similar, but the systematics limit of Setup 2 is slightly better (cf., Figure 2). For a normal hierarchy, the discovery reach of Setup 3 covers considerably less parameter space than that one of a neutrino factory at  $L = 3000$  km. For the inverted hierarchy, the matter effect enhancement of the lower neutrino factory anti-neutrino rate (instead of the higher neutrino rate) leads to a relatively degraded reach for the neutrino factory baselines, whereas the event numbers of the  $\beta$ -beams are rather similar for neutrinos and anti-neutrinos. However, the neutrino factory at 3000 km covers the most parameter space in both cases, and the superbeam upgrade T2HK\* by far the least. Note that the neutrino factory behavior for the  $\sin^2 2\theta_{13}$

<sup>4</sup>This behaviour could in principle change once additional information like  $\nu_\tau$  appearance is available

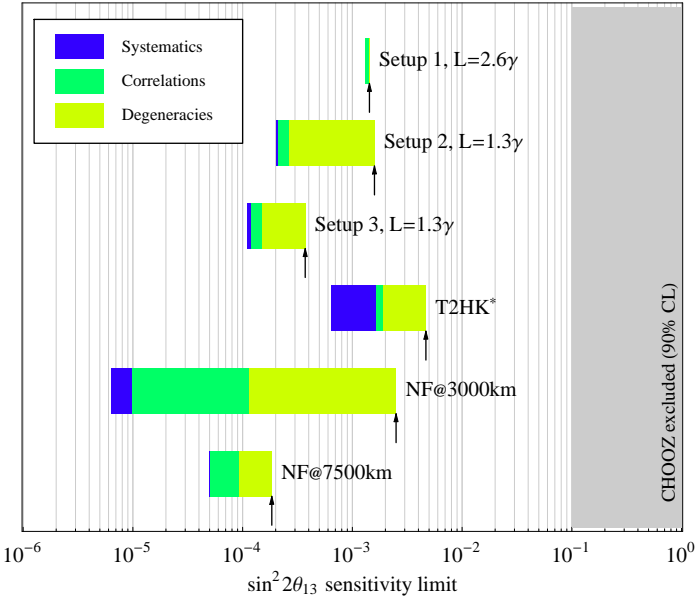


**Figure 6:** The  $\sin^2 2\theta_{13}$  sensitivity limits for the different setups and other representatives. Here  $n = 0$  (decays per year fixed) and the  $3\sigma$  confidence level are chosen. The final sensitivity limits are obtained as the right edges of the bars after successively switching on systematics, correlations, and degeneracies.

sensitivity and  $\sin^2 2\theta_{13}$  discovery reach is completely different. For the  $\sin^2 2\theta_{13}$  sensitivity, very few particular combinations of parameters prevent a strong  $\sin^2 2\theta_{13}$  limit, whereas for the  $\sin^2 2\theta_{13}$  discovery reach, correlations and degeneracies are of secondary importance. A neutrino factory is therefore clearly a  $\sin^2 2\theta_{13}$  discovery machine. Note that the discovery reach fit rate vector is computed for (fixed)  $\sin^2 2\theta_{13} = 0$ , which means there is only a substantial impact of correlations if the solar appearance term contributes significantly to the appearance rate.<sup>5</sup> Since the solar appearance term does not depend on the mass hierarchy, there is no contribution of the  $\text{sgn}(\Delta m_{31}^2)$ -degeneracy.

In summary, all of the discussed  $\beta$ -beam options could be interesting alternatives to a superbeam upgrade or intermediate options towards a neutrino factory. Especially Setup 1, which uses the identical detector needed for other applications, might be an interesting transition candidate. Since the  $\beta$ -beams have a clean composition of electron neutrinos, they are not affected by an intrinsic contamination of muon events and are therefore not systematics limited close to  $\sin^2 2\theta_{13} \sim 10^{-3}$  such as superbeams are. We will discuss the sensitivity to the mass hierarchy and CP violation in the next section in order to get a broader perspective of the problem, and to evaluate if a  $\beta$ -beam could, in principle, replace a neutrino factory.

<sup>5</sup>It turns out that these correlations have some impact on the discovery reach of Setup 1 and the neutrino factory baselines, especially  $L = 3\,000$  km, since both, having a long enough baseline and being far off the matter density resonance (in energy) increase the relative importance of the solar appearance term.

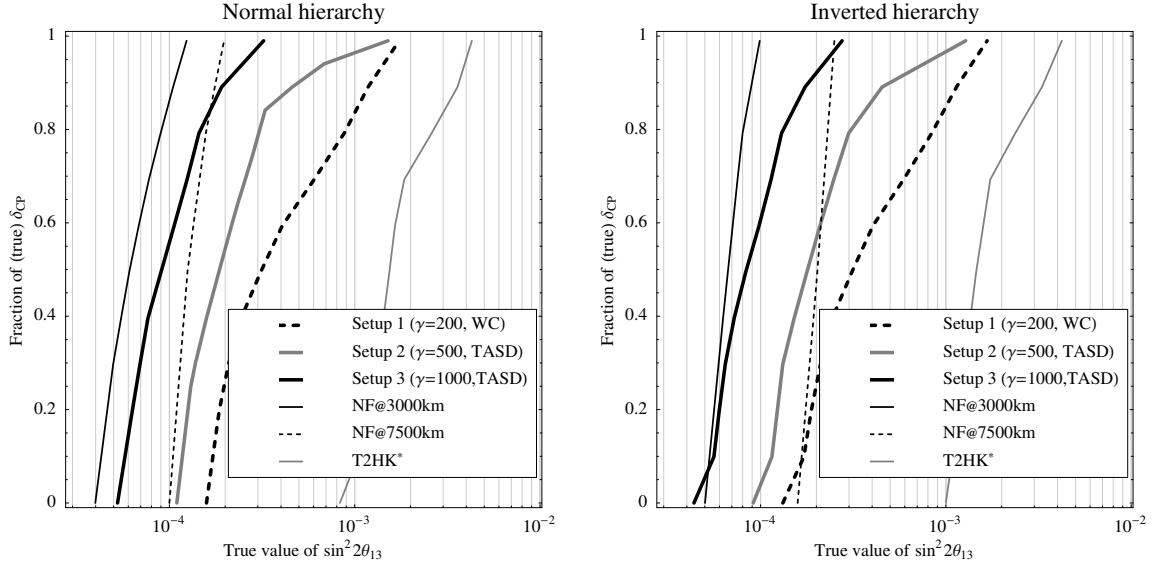


**Figure 7:** The  $\sin^2 2\theta_{13}$  discovery reach (including systematics and correlations) for different setups as function of the true values of  $\sin^2 2\theta_{13}$  and  $\delta_{\text{CP}}$  ( $3\sigma$  confidence level), where the left plot is for the normal hierarchy and the right plot for the inverted hierarchy. The values of  $\delta_{\text{CP}}$  are “stacked” to the fraction of  $\delta_{\text{CP}}$ , *i.e.*,  $\sin^2 2\theta_{13}$  will be discovered for a certain fraction of all possible values of  $\delta_{\text{CP}}$ . For a uniform probability contribution in  $\delta_{\text{CP}}$ , the fraction of  $\delta_{\text{CP}}$  directly corresponds to the probability to discover  $\sin^2 2\theta_{13}$ .

## 4 Sensitivity to mass hierarchy and CP violation

Beyond detecting a finite value of  $\sin^2 2\theta_{13}$ , the mass hierarchy and CP violation sensitivities are the two most interesting quantities to be measured by the discussed experiments. We will first introduce performance indicators for these quantities. Then we will discuss optimization aspects for the mass hierarchy and CP violation determination. Finally, we will compare the performances of the  $\beta$ -beam setups with other experiments.

### 4.1 Performance indicators

We define sensitivity to a particular mass hierarchy (normal or inverted) if the wrong-sign solution can be excluded at a certain confidence level. This implies that a  $\text{sgn}(\Delta m_{31}^2)$ -degeneracy [48] or mixed degeneracy [51] will destroy the mass hierarchy sensitivity. The mass hierarchy sensitivity does not only depend on the simulated hierarchy, but also on the true values of  $\sin^2 2\theta_{13}$  and  $\delta_{\text{CP}}$ . Since it is not possible to show the full parameter space for mass hierarchy sensitivity simultaneously, we use in many cases the sensitivity for the true  $\delta_{\text{CP}} = 0$ . In other cases, we show the mass hierarchy sensitivity as function of  $\sin^2 2\theta_{13}$  and  $\delta_{\text{CP}}$ , where we stack the true values of  $\delta_{\text{CP}}$  to the “Fraction of  $\delta_{\text{CP}}$ ” (CP fraction) similar to Figure 7. A mass hierarchy sensitivity for a CP fraction 1 corresponds to mass hierarchy sensitivity for any values of  $\delta_{\text{CP}}$  (worst case in  $\delta_{\text{CP}}$ ), and a mass hierarchy sensitivity for

a CP fraction  $\rightarrow 0$  to mass hierarchy sensitivity for the best case  $\delta_{\text{CP}}$ . A CP fraction 0.5 refers to the “typical” value of  $\delta_{\text{CP}}$ , *i.e.*, 50% of all cases of  $\delta_{\text{CP}}$ . Note that the CP fraction is a probabilistic measure in the sense that only one of these values can be realized by nature. Assuming a uniform distribution of  $\delta_{\text{CP}}$ , it directly corresponds to the probability to discover the mass hierarchy for a chosen  $\sin^2 2\theta_{13}$ .

We define sensitivity to CP violation if the CP conserving solutions  $\delta_{\text{CP}} = 0$  and  $\delta_{\text{CP}} = \pi$  can be excluded at a certain confidence level. This implies that any degenerate solution overlapping a CP conserving solution destroys the sensitivity to CP violation. Note that this sensitivity clearly differs from the parameter sensitivity to a specific parameter value of  $\delta_{\text{CP}}$ , which includes the sensitivity to the special value  $\delta_{\text{CP}} = 0$ . In some cases, we only show the parameter sensitivity to maximal CP violation  $\delta_{\text{CP}} = \pi/2$  or  $\delta_{\text{CP}} = 3\pi/2$ . However, since any value of  $\delta_{\text{CP}} \neq \{0, \pi\}$  violates CP, we also show the parameter sensitivity to any CP violation in other cases, *i.e.*, the sensitivity to CP violation as function of the true values of  $\sin^2 2\theta_{13}$  and  $\delta_{\text{CP}}$  (which, in principle, also depends on the simulated mass hierarchy). Similar to the mass hierarchy sensitivity, we then stack the values of  $\delta_{\text{CP}}$  to the “Fraction of  $\delta_{\text{CP}}$ ”. Note, however, that no experiment can have a CP fraction 1.0 for the CP violation sensitivity at any point, since there will be no CP violation sensitivity for values of  $\delta_{\text{CP}}$  close to 0 and  $\pi$ .

## 4.2 Scaling with $\gamma$ and optimization

Similar to the  $\sin^2 2\theta_{13}$  sensitivity, one can discuss the mass hierarchy and CP violation sensitivities as function of  $\gamma$  for the different detector technologies. This comparison is shown in Figure 8 for the chosen range of  $L/\gamma$ . Since higher  $\gamma$  implies a longer baseline, it also implies stronger matter effects, where we use the average density along a specific baseline. Therefore the mass hierarchy sensitivity also improves with higher values of  $\gamma$  (*cf.*, left plot). The different choice of  $L/\gamma$  for the WC detector implies that the mass hierarchy sensitivity is already present at about half of the  $\gamma$  for the TASD. There is no substantial difference between the normal and inverted mass hierarchies, because all setups use approximately equal neutrino and anti-neutrino rates. For the CP violation sensitivity, higher  $\gamma$ ’s are, in principle, favorable, since they imply larger event rates. However, for very high  $\gamma$ , the missing energy resolution of the non-QE events (WC) and the matter density uncertainties (TASD) act counter-productive. For the  $\beta$ -beams, there seem to exist only very little problems with degeneracies for the CP violation sensitivity, because the measurement at the oscillation maximum helps to resolve the degeneracies.

It is interesting to discuss what the choices of  $L/\gamma$  for Setups 1, 2, and 3 are really optimized for. So far, we have demonstrated that the choice of  $L/\gamma = 2.6$  for the WC detector and  $L/\gamma = 1.3$  for the TASD are quasi-optimal for the  $\sin^2 2\theta_{13}$  sensitivity and lead to a clear hierarchy of these setups for the  $\sin^2 2\theta_{13}$  discovery reach. We show in Figure 9 the  $L/\gamma$ -dependence for all three setups and the  $\sin^2 2\theta_{13}$  sensitivity (black solid curves), maximal CP violation sensitivity (dashed curves), and normal mass hierarchy sensitivity for  $\delta_{\text{CP}} = 0$  (gray curves). The thick vertical lines correspond to our choices of  $L/\gamma$ , whereas the thin lines represent alternative optimization strategies. Setup 1 is apparently optimized for the  $\sin^2 2\theta_{13}$  sensitivity, where the large  $L/\gamma$  clearly favors the mass hierarchy sensitivity and

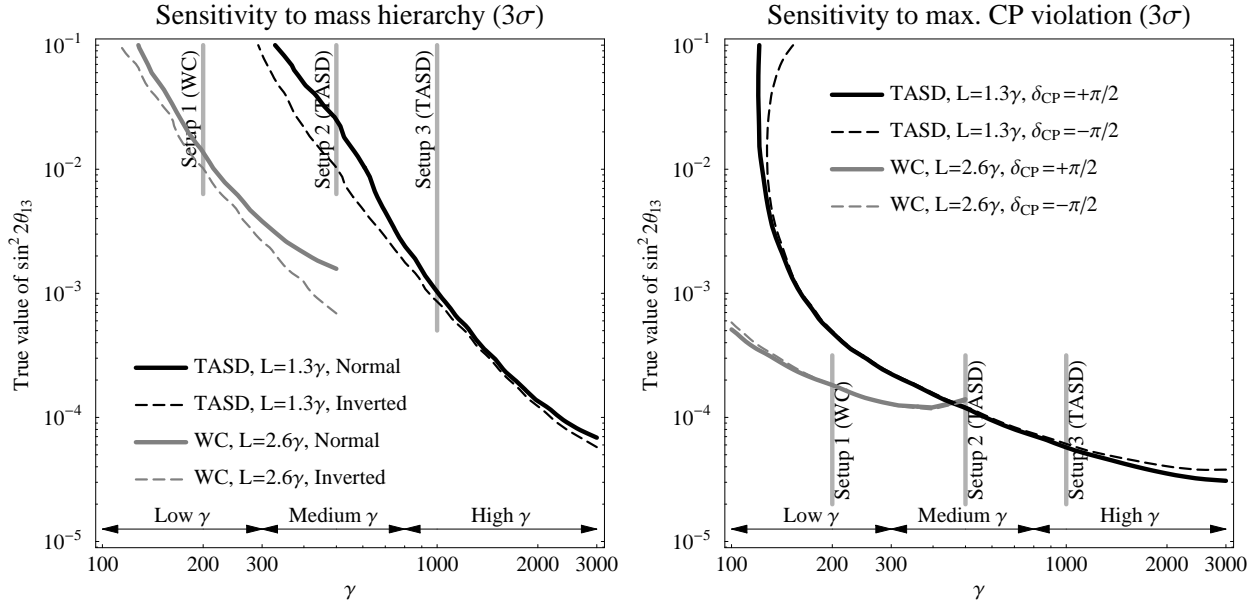


**Figure 8:** The sensitivity to the mass hierarchy (left,  $\delta_{CP} = 0$ ) and maximal CP violation (right, normal hierarchy) as function of  $\gamma$  and the true value of  $\sin^2 2\theta_{13}$  for the detector types and parameters as described in the plot legends, where sensitivity at the  $3\sigma$  confidence level is given above the curves.

hardly affects the CP violation sensitivity. Thus, it represents a good compromise for all quantities. Setups 2 and 3 are optimized for CP violation, where the  $\sin^2 2\theta_{13}$  sensitivity is in both cases very close to the optimum. For Setups 2 and 3, however, the mass hierarchy sensitivity would be considerably better close to the second oscillation maximum  $L/\gamma \sim 2.6$ , while the  $\sin^2 2\theta_{13}$  sensitivity would be hardly degraded. The choice of the baseline depends therefore for Setups 2 and 3 on the priorities, *i.e.* if one optimizes for mass hierarchy or CP violation measurements. Since we also use the setup NF@7500km for the neutrino factory, we will show Setups 2 and 3 at the second oscillation maximum in some cases for a fair comparison of the mass hierarchy sensitivity. Note that Setup 3 could, in principle, also be operated at the “magic baseline”, where the mass hierarchy and  $\sin^2 2\theta_{13}$  sensitivities are only somewhat worse than optimal, but no CP violation measurement is possible. The only quantity which is not shown here is the  $\sin^2 2\theta_{13}$  discovery reach. One can show that it is substantially degraded for the second oscillation maximum at Setups 2 or 3 ( $L = 2.6\gamma$ ). In particular, Setup 2 would perform much worse than Setup 1. However, the choice of the first oscillation maximum instead of the second would hardly change the parameter space coverage of Setup 2. Thus, our choices of  $L/\gamma$  are consistent with the primary objective to discover  $\sin^2 2\theta_{13}$ .

Recently the important issue has been raised that the neutrino event rates might be substantially suppressed compared to the anti-neutrino event rates. We show therefore in Figure 10 the dependence on the neutrino running fraction for all three setups and the  $\sin^2 2\theta_{13}$  sensitivity (black solid curves), maximal CP violation sensitivity (dashed curves), and normal mass hierarchy sensitivity for  $\delta_{CP} = 0$  (gray curves). The vertical thick lines correspond to our choice of 50% neutrino and 50% anti-neutrino running. The neutrino running fraction

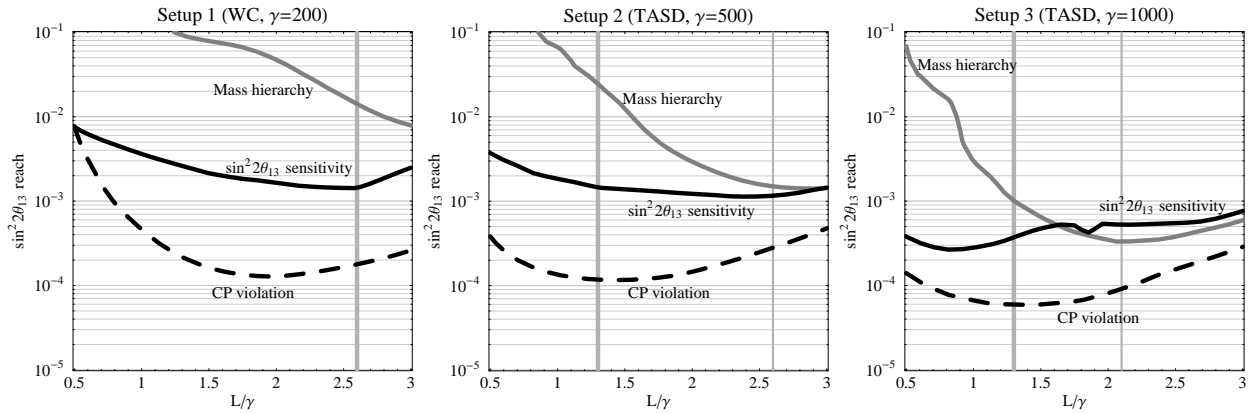


**Figure 9:** The  $\sin^2 2\theta_{13}$  reaches for the sensitivity to  $\sin^2 2\theta_{13}$  (black solid curves), maximal CP violation  $\delta_{\text{CP}} = \pi/2$  (dashed curves), and the normal mass hierarchy for  $\delta_{\text{CP}} = 0$  (gray solid curves) as function of  $L/\gamma$  for the different scenarios in the figure captions (3 $\sigma$  confidence level). The thick vertical lines correspond to the scenarios chosen in this study. The thin vertical lines correspond to alternative optimization strategies. All these curves include correlations and degeneracies.

$f$  is the fraction of neutrino running divided by the total running time of eight years, *i.e.* the experiment runs  $f \times 8$  years with neutrinos and  $(1 - f) \times 8$  years with anti-neutrinos. From Figure 10, we find that all setups are at the optimal performance for the CP violation measurements (vertical lines). Setups 1 and 2 also have optimal  $\sin^2 2\theta_{13}$  sensitivity, whereas Setup 3 has optimal mass hierarchy sensitivity. As far as the symmetry of the plots is concerned, running with only anti-neutrinos is clearly favored compared to running with only neutrinos (extreme cases), because we have somewhat higher anti-neutrino event rates and lower backgrounds, *i.e.* the absolute rate is higher for the anti-neutrino case. For the inverted hierarchy (Figure 10 is shown for the normal hierarchy), only running with neutrinos is even slightly more disfavored because of the matter suppression of the neutrino rate. It is interesting to note that even rather substantial deviations from a symmetric neutrino and anti-neutrino operation does not have extreme effects on the measurements. Setup 3 is most affected by such deviations, where a lower neutrino fraction means better statistics and thus a better  $\sin^2 2\theta_{13}$  sensitivity, but it creates an imbalance between neutrinos and anti-neutrinos affecting the CP violation sensitivity. Nevertheless, it does not make sense to run with neutrinos or anti-neutrinos only, since this ratio would lead to degrading the sensitivities by an order of magnitude. Setup 1, for example, then loses its competitiveness compared to superbeam upgrades. In all cases, at least 10%-20% of neutrino running is necessary, which corresponds rescaled to at least a total number of  $1 \cdot 10^{18}$  useful  $^{18}\text{Ne}$  decays plus  $26 \cdot 10^{18}$  useful  $^6\text{He}$  decays.

### 4.3 Comparison with other technologies

In Figure 11 the sensitivity to CP violation is shown for the normal (left) and inverted (right) mass hierarchy for different experiments as function of the true values of  $\sin^2 2\theta_{13}$  and  $\delta_{\text{CP}}$  at the 3 $\sigma$  confidence level. This figure clearly demonstrates that for a normal mass hierarchy

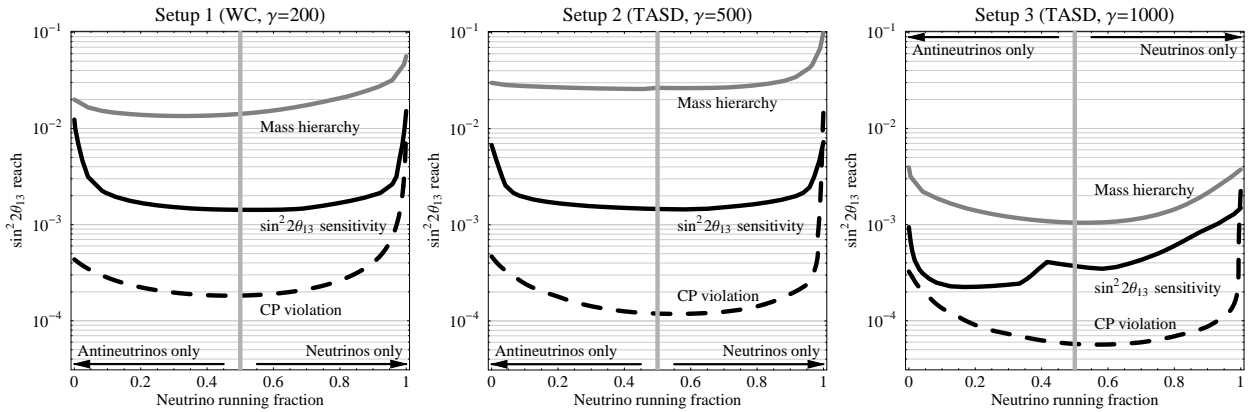


**Figure 10:** The  $\sin^2 2\theta_{13}$  reaches for the sensitivity to  $\sin^2 2\theta_{13}$  (black solid curves), maximal CP violation  $\delta_{CP} = \pi/2$  (dashed curves), and the normal mass hierarchy for  $\delta_{CP} = 0$  (gray solid curves) as function of the neutrino running fraction for the different scenarios in the figure captions (3 $\sigma$  confidence level). The neutrino running fraction is the neutrino running time divided by the total running time of eight years. The thick vertical lines correspond to the scenarios chosen in this study. All these curves include correlations and degeneracies and are computed for the normal mass hierarchy.

all of the discussed  $\beta$ -beam options have an impressive CP violation sensitivity very competitive to the neutrino factory, because  $(\delta_{CP}, \sin^2 2\theta_{13})$ -degeneracy [47] and “ $\pi$ -transit” of the  $\text{sgn}(\Delta m_{31}^2)$ -degeneracy [29] destroy the CP violation sensitivity of the neutrino factory at many places. Note that these degeneracy problems could, in principle, be resolved by a combination with the magic baseline, but a much better sensitivity than that of Setup 3 is unlikely to be achieved. As far as the  $\sin^2 2\theta_{13}$  reach is concerned (in horizontal direction), there is again a clear hierarchy among Setups 1, 2, and 3. For large values of  $\sin^2 2\theta_{13}$ , however, matter density uncertainties affect the longer baselines, and Setup 2 has to deal with some problems due to degeneracies (left plot). For optimal  $\sin^2 2\theta_{13}$ , Setup 3 can establish CP violation for more than 90% of all values of  $\delta_{CP}$ , whereas the neutrino factory is limited to about 80%. For the inverted hierarchy, the matter effects enhance the anti-neutrino rate, which means that the neutrino and (lower) anti-neutrino rates at the neutrino factory are getting more equal statistical weight and the correlations can easier be resolved. Balanced event rates of the  $\beta$ -beams lead, on the other hand, to very little impact of the mass hierarchy. For T2HK\*, the somewhat lower anti-neutrino rate implies a similar behavior to the neutrino factory.

In order to compare the mass hierarchy sensitivity of all options, we show in Figure 12 the mass hierarchy sensitivity as function of  $\sin^2 2\theta_{13}$  and  $\delta_{CP}$  for the normal (left) and inverted (right) mass hierarchy for the Setups defined in the last section and the neutrino factory and superbeam representatives. Given the choice of  $L/\gamma$ , Setups 1 and 2 have a very similar mass hierarchy sensitivity because of the very similar baselines, whereas Setup 3 is substantially better. In all cases, the neutrino factory at the magic baseline covers by far the most parameter space, whereas the performance of NF@3000km is very close to the one of Setup 3. The superbeam setup T2HK\* can only establish the mass hierarchy for a very small fraction of  $\delta_{CP}$  because of its short baseline. Note, however, that other superbeam upgrades

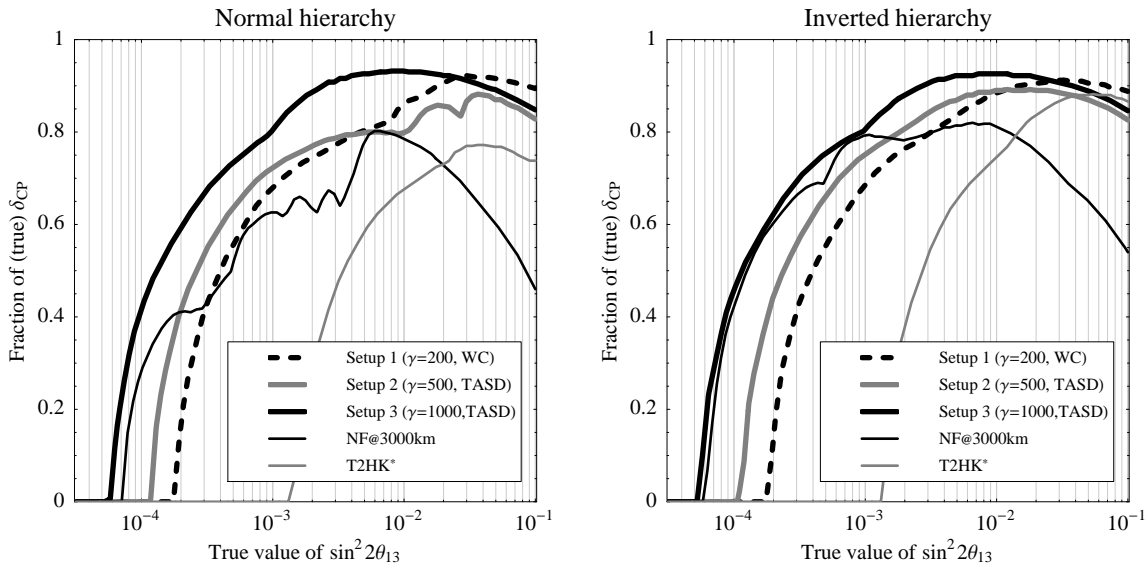


**Figure 11:** The sensitivity to CP violation for the normal (left) and inverted (right) mass hierarchy for different experiments as function of the true values of  $\sin^2 2\theta_{13}$  and  $\delta_{\text{CP}}$  at the  $3\sigma$  confidence level. The values of  $\delta_{\text{CP}}$  are “stacked” to the CP fraction, which described the fraction of all values of  $\delta_{\text{CP}}$  for which the mass hierarchy can be resolved for a given  $\sin^2 2\theta_{13}$ . If the probability distribution is uniform in  $\delta_{\text{CP}}$ , the fraction of  $\delta_{\text{CP}}$  would directly correspond to the probability to measure the indicated mass hierarchy for a given  $\sin^2 2\theta_{13}$ .

(such as FNAL-Homestake or BNL-Homestake) could have a much better mass hierarchy sensitivity [52]. The relative performance of the neutrino factory baselines is degraded for the inverted versus normal hierarchy, because the event rates are not evenly distributed between neutrinos and anti-neutrinos. As we have discussed in the last section, a longer baseline for Setups 2 and 3 improves the mass hierarchy sensitivity drastically. It turns out that for  $L/\gamma = 2.6$ , Setup 2 is comparable to the neutrino factory at 3000 km, whereas Setup 3 is almost as good as the neutrino factory at the magic baseline.

A very interesting (though not very likely) case for the  $\beta$ -beams could occur if  $\Delta m_{31}^2$  turns out to be at the lower end of the currently allowed 90% CL region [27], *i.e.*,  $\Delta m_{31}^2 \simeq 0.0015 \text{ eV}^2$ . Since  $\Delta m_{31}^2$  will be measured to a high precision soon by MINOS, T2K, and NO $\nu$ A, it is straightforward to re-optimize the  $\beta$ -beams by just moving the detector back into the oscillation maximum. For the neutrino factory, however, the oscillation maximum for the mean energy is at a very long baselines  $L \gg 7500 \text{ km}$  anyway, which means that moving the detector to an even longer baseline should have an effect similar to choosing the magic baseline scenario directly. In addition, other constraints may prevent the selection of longer baselines. We illustrate the effect of a smaller  $\Delta m_{31}^2$  in Figure 13, where the arrows indicate the shift. In this figure, the  $\beta$ -beam baselines are re-scaled according to  $L \rightarrow L \times 0.0025/0.0015$  in order to stay in the oscillation maximum, whereas the other baselines are fixed. In almost all cases the experiments loose sensitivity. However, the relative shift for the neutrino factories is in some cases much larger because the smaller  $\Delta m_{31}^2$

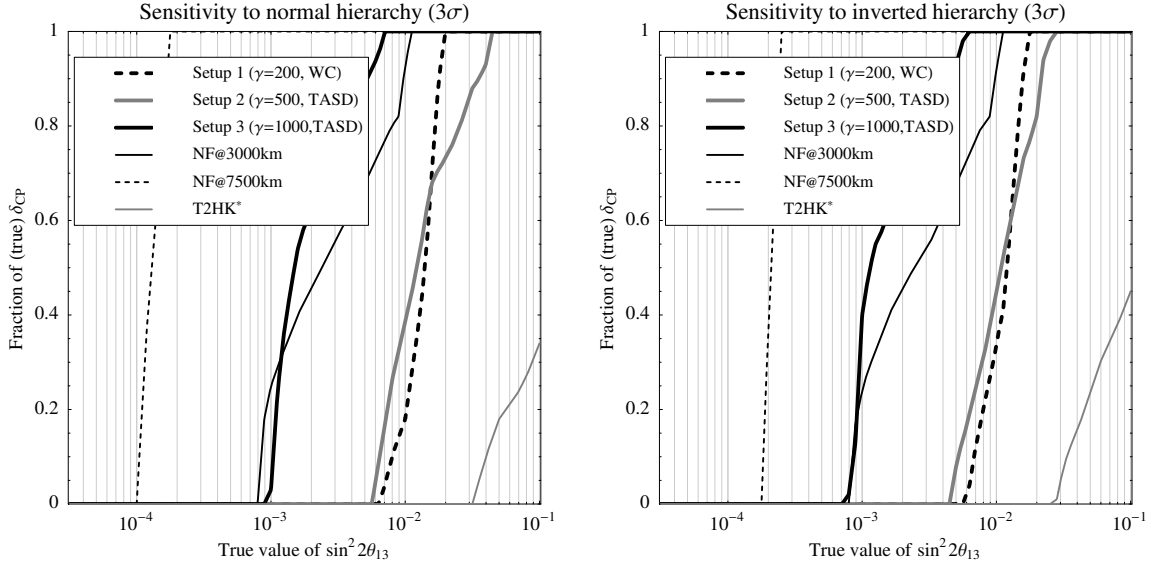


**Figure 12:** The sensitivity to a normal (left) and inverted (right) mass hierarchy for different experiments as function of the true values of  $\sin^2 2\theta_{13}$  and  $\delta_{\text{CP}}$  at the  $3\sigma$  confidence level. The values of  $\delta_{\text{CP}}$  are “stacked” to the CP fraction, which describes the fraction of all values of  $\delta_{\text{CP}}$  for which the mass hierarchy can be resolved for a given  $\sin^2 2\theta_{13}$ . If the probability distribution was uniform in  $\delta_{\text{CP}}$ , the fraction of  $\delta_{\text{CP}}$  would directly correspond to the probability to measure the indicated mass hierarchy for a given  $\sin^2 2\theta_{13}$ .

means that the oscillation peak is shifted to lower energies where the charge identification requirement leads to lower efficiencies. In particular, the CP violation sensitivity of the neutrino factory is highly affected. For the mass hierarchy sensitivity, the neutrino factory at the magic baseline is still the best experiment. Note that Setups 1 and 2 are hardly affected by the different value of  $\Delta m_{31}^2$ , since a smaller value of  $\Delta m_{31}^2$  means a longer baseline and the stronger matter effects partially (Setup 2) or fully (Setup 1) compensate for the drop in  $1/L^2$ . To be fair, this comparison is only shown for selected parameter choices and for the assumption of unflexible neutrino factory baselines. Indeed, for a smaller value of  $\Delta m_{31}^2$ , a dedicated study is required which re-optimizes all potential experiments. However, one can easily see from this figure that the charge identification cuts at low energies for the neutrino factory imply that one quickly ends up at inconveniently long baselines for such an optimization. This behavior is not expected for the  $\beta$ -beams.

## 5 Summary and conclusions

In this study, we have discussed various optimization aspects of  $\beta$ -beams and we compared the physics potential to neutrino factories and superbeam upgrades. Two central parameters are the gamma factor and the baseline of the  $\beta$ -beam which were taken to be free parameters. We considered two different detector technologies in connection with the  $\beta$ -beam, namely a Water Cherenkov detector and a Totally Active Scintillator Detector with 500 kt and 50 kt

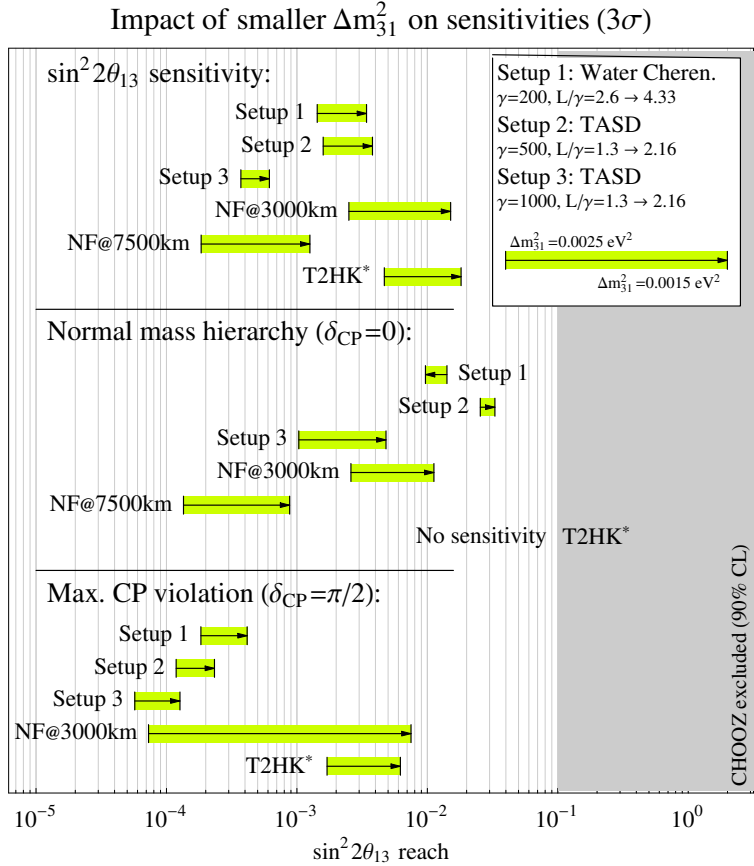


**Figure 13:** Impact of a smaller value of  $\Delta m_{31}^2$  on different sensitivities of various experiments including all correlations and degeneracies ( $3\sigma$  confidence level). The bars represent the shift from  $\Delta m_{31}^2 = 0.0025 \text{ eV}^2 \rightarrow \Delta m_{31}^2 = 0.0015 \text{ eV}^2$  (simulated values), where the  $\beta$ -beam baselines are re-scaled according to  $L \rightarrow L \times 0.0025/0.0015$ . Note that for the CP violation sensitivity in this figure, we have chosen the smallest value of  $\sin^2 2\theta_{13}$  for which maximal CP violation could be established.

fiducial mass, respectively. The Water Cherenkov detector was also considered as a target for a superbeam upgrade which we called T2HK\*. For the comparison with the neutrino factory we used a 50 kt magnetized iron detector at baselines of 3000 km and 7500 km. An important aspect concerns the assumptions about the number of ion decays per year. One scenario was to assume that the number of decays does not depend on  $\gamma$ . However, this is for a number of reasons technologically not realistic and we studied therefore scenarios where the number of decays per year scales with  $\gamma$  like a power law. For the superbeam upgrade and the neutrino factory “standard” beam luminosities were assumed (see section 3.4 for details). As performance indicators, we have considered the  $\sin^2 2\theta_{13}$  sensitivity (corresponding to the exclusion limit which can be achieved by an experiment), the  $\sin^2 2\theta_{13}$  discovery reach, the (normal and inverted) mass hierarchy discovery reach, and the CP violation discovery reach for both hierarchies. Specific experimental setups were defined to allow a more detailed comparison.

Our main results for the discovery reaches are summarized in Figure 14, where the bands

reflect the impact of the true value of  $\delta_{\text{CP}}$ . We find that the choice of the optimal  $\gamma$  clearly depends on the objectives of the  $\beta$ -beam experiment and external constraints. We in general find good agreement with existing studies showing that  $\gamma$  should be at least high enough to avoid the Fermi-motion dominated regime in order to have sufficient energy information [10, 16]. Low  $\gamma \lesssim 300$  can be achieved with relatively “small” accelerators, such as of SPS size in combination with Water Cherenkov detectors. All of the discussed performance indicators imply that a  $\beta$ -beam in this range clearly outperforms the T2HK\* superbeam upgrade using the same detector since it is not limited by the intrinsic beam background. In fact, the CP violation discovery reach is already quite close to the optimum even compared with higher gamma or neutrino factory setups. Note that this excellent simultaneous sensitivity to  $\sin^2 2\theta_{13}$ , mass hierarchy, and CP violation is achieved by including the second oscillation maximum to disentangle correlations and degeneracies. An operation at a shorter baseline would significantly affect the final mass hierarchy and  $\sin^2 2\theta_{13}$  sensitivities, and it would hardly help the CP violation sensitivity. Note that we have chosen the ion decay rates such that there are approximately equal neutrino and anti-neutrino event rates for all setups. This balanced concept implies that the  $\beta$ -beam performance hardly depends on the mass hierarchy and the performance for CP violation is excellent. However, if the neutrino rate were significantly lower than the anti-neutrino rate, then the CP violation sensitivity would be affected.

The range  $300 \lesssim \gamma \lesssim 800$ , requires already relatively large accelerator rings, such as of Tevatron size. As detector technology, we have chosen the Totally Active Scintillator Detector (TASD) in this case, because it is rather predictable in this gamma-range. However, it is not excluded that the extrapolation to a ten times larger Water Cherenkov could result in a better performance. For the setup in this and the larger gamma range, we find that the choice of  $L/\gamma = 1.3$  or  $2.6$  clearly depends on the optimization goals. For  $\sin^2 2\theta_{13}$  discovery and CP violation potential, shorter baselines are favored, whereas sensitivity to the mass hierarchy favours longer baselines. The  $\sin^2 2\theta_{13}$  is rather indifferent with respect to the baseline choice, since statistics becomes worse for longer baselines, while the matter effects become stronger and the second oscillation maximum helps to resolve correlations and degeneracies. Except for CP violation, even the optimized medium  $\gamma$  setup is not competitive to the neutrino factory, but it could be an interesting step towards it.

Large  $\gamma \gtrsim 800$  would require very large and powerful accelerators of LHC size, where we use TASD as detector technology. We find  $\sin^2 2\theta_{13}$  (sensitivity and discovery) and mass hierarchy discovery reaches close to the neutrino factory setups, and a CP violation discovery reach better than the one of the neutrino factory setups (*cf.*, Figure 6 and Figure 14). In this case, a  $\beta$ -beam could clearly be a competitor to a neutrino factory, if technically feasible for such a high  $\gamma$ .

We have assumed initially that the number of ion decays per year is constant in  $\gamma$  and we investigated the impact of external constraints to this assumption. We found that especially the high gamma setup suffers from modifications in the scaling of ion decays. This implies that the ion luminosity is a critical factor for this setup. In addition, we compare in Figure 14 setups optimal for the individual purposes, *i.e.*, differently optimized  $\beta$ -beams with correspondingly optimized neutrino factories. If we required optimal sensitivity to all quantities, we would need two neutrino factory or two  $\beta$ -beam baselines. Though

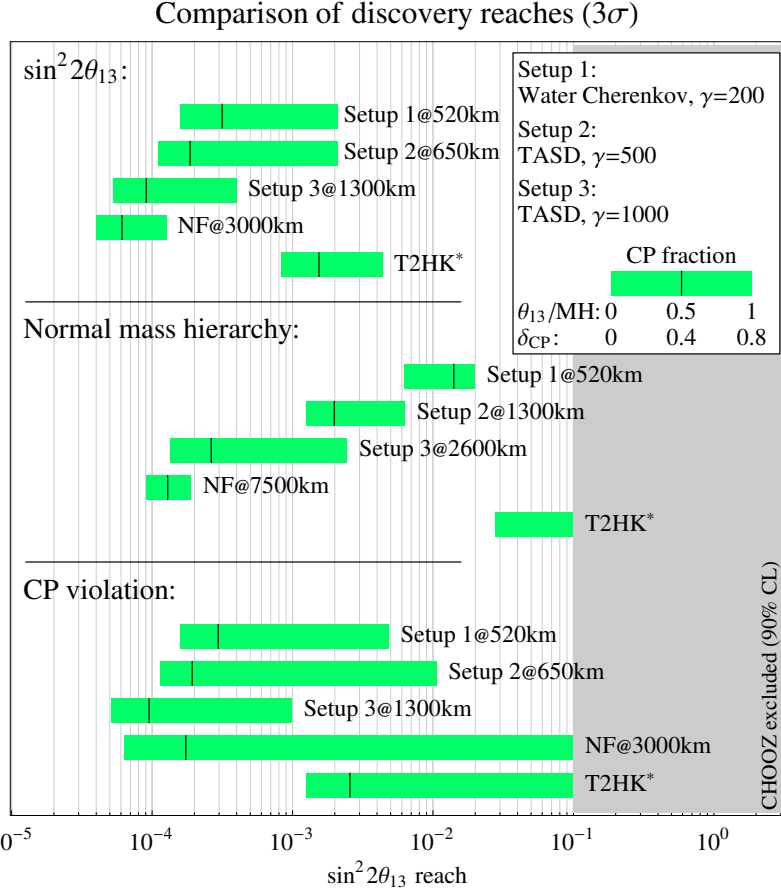


**Figure 14:** Discovery reach comparison at the  $3\sigma$  confidence level. The bars represent the best case (left end), “typical case” (middle line), and worst case (right end) in  $\delta_{CP}$ , where the respective sensitivities are computed with the CP fractions in the plot legend. Note that for CP violation, a CP fraction of one can never be achieved since values close to 0 or  $\pi$  cannot be distinguished from CP conservation. Within each category, the most competitive setups from this study are compared (first or second oscillation maximum for  $\beta$ -beams). For all shown sensitivities, a normal mass hierarchy is assumed.

a storage ring with two decay sections could, in principle, be possible for a  $\beta$ -beam, it might be more compact in the neutrino factory case. If, however, one of the measurements becomes obsolete, such as the mass hierarchy which might be determined by a supernova explosion, the  $\beta$ -beam baseline optimization seems to be quite straightforward, whereas the neutrino factory may still require another baseline to resolve degeneracies. For a precision measurement of  $\delta_{CP}$ , for example, the “magic baseline” could be required for unfortunate values of  $\delta_{CP}$  [53].

The  $\beta$ -beam has in all cases the advantage that the baseline can be freely chosen such that one is measuring at the oscillation maximum. For the case of a much smaller  $\Delta m_{31}^2$  than the current best-fit value, first tests suggest that the performance improves compared to neutrino factories. However, this less likely case requires further study because one should also optimize the neutrino factory for such a different value of  $\Delta m_{31}^2$ .

We conclude that a lower gamma  $\beta$ -beam is certainly an interesting physics alternative to a large superbeam upgrade and a higher gamma  $\beta$ -beam could be an competitive alternative to a neutrino factory. In all cases, the attractiveness of the  $\beta$ -beams depends clearly on the ability to produce enough isotope decays for both neutrinos and anti-neutrinos. Especially for  $\delta_{\text{CP}}$  measurements, the  $\beta$ -beams might then outperform all existing techniques, whereas for  $\sin^2 2\theta_{13}$  discovery and mass hierarchy sensitivity the neutrino factory is ultimately a better choice. Except from  $\sin^2 2\theta_{13}$ , mass hierarchy, and CP violation measurements, there is more physics to be done with a neutrino factory. In the neutrino oscillation sector, for example, there is sensitivity to the leading atmospheric parameters. The case  $\sin^2 2\theta_{13} = 0$  would suggest to use the  $\nu_\mu$  disappearance channel at a very long baseline for mass hierarchy and MSW effect measurements [54, 55]. This role is unlikely to be replaced by the electron neutrino disappearance channel of a  $\beta$ -beam. Nevertheless, we conclude that  $\beta$  beams constitute a very interesting option for future precision neutrino oscillation experiments. Further technological feasibility studies are clearly well motivated to explore if a  $\beta$  beam can be realized. The technical feasibility, the financial effort, and the physics potential of a  $\beta$ -beam and a neutrino factory have to be compared then again before an ultimate decision is made.

## Acknowledgments

We would like to thank M. Lindroos, P. Litchfield, M. Mezzetto, and L. Mualem for useful information. This work has been supported by SFB 375 and the Graduiertenkolleg 1054 of Deutsche Forschungsgemeinschaft. WW would like to acknowledge support from the W. M. Keck Foundation and NSF grant PHY-0070928. In addition, he would like to thank the theory groups at TUM and Wisconsin for their warm hospitality during his visits, where parts of this work have been carried out.

## Appendix A: Water Cherenkov detector and 2nd oscillation maximum

The better performance of Setup 1 at the longer baseline with  $L/\gamma = 2.6$  (although statistics drops with  $1/L^2$ ) can be understood with Figure 15 where the comparison of  $L/\gamma = 1.3$  (left column) and  $L/\gamma = 2.6$  (right column) is shown. The appearance spectra for  $\sin^2 2\theta_{13} = 0.01$  and  $\delta_{CP} = \pi/4$  is shown in the first row of Figure 15 for neutrinos (black curve) and anti-neutrinos (gray curve). For Setup 1 at  $L/\gamma = 1.3$  one can clearly see, that only the first oscillation maximum contributes to the whole appearance spectra, while for the one at  $L/\gamma = 2.6$  the first oscillation appearance maximum is shifted to higher neutrino energies and appearance events from the second oscillation maximum enter the energy window of the analysis from lower energies but the overall event rates are decreased. In the second row, we show the allowed regions in the  $\theta_{13}$ - $\delta$  plane at 1, 2, and 3  $\sigma$  for the same true oscillation parameters (indicated by the black dot) where only systematical errors are taken into account. The allowed regions for the  $L/\gamma = 2.6$  scenario are somewhat larger due to the lower statistics. But only if also correlations and degeneracies are included (third row) one can see the impact of the second oscillation maximum. The degenerate solution fitted with  $\Delta m_{31}^2 < 0$  is smaller for the  $L/\gamma = 2.6$  scenario and does not reach to higher values of  $\theta_{13}$  than the region that contains the best-fit value. Additionally the  $\Delta\chi^2$  value at the local minimum of the degenerate solution is much higher with  $L/\gamma = 2.6$  than the one with  $L/\gamma = 1.3$  and does not even appear at 1  $\sigma$ .

In order to understand better the impact of the appearance events from the second oscillation maximum in the  $L/\gamma = 2.6$  scenario, we divided the whole data set of Setup 1 in two separate data sets which only contain the appearance events from the first or second oscillation maximum. Data set I reaches from 0.2 to 0.7 GeV and data set II reaches from 0.7 to 1.6 GeV as can be seen in the upper right picture of Figure 15. In Figure 16 we compare again the allowed regions in the  $\theta_{13}$ - $\delta$  plane at 1, 2, and 3  $\sigma$ , now for data set I (left column), data set II (middle column) and both data sets combined (right column). In the first row we only consider systematics and in the second row correlations and degeneracies are switched on. One can clearly see that due to extremely low statistics with only the appearance events from data set 1 the allowed regions are strongly expanded. The allowed regions from data set II are highly improved and in the case "systematics only" even somewhat smaller than for the combination of both data sets. This effect comes from the fact that most of the background events reconstruct at smaller energies (i.e. within data set I) and therefore the S/B ratio is smaller for data set I only. But for the degenerate solution fitted with  $\Delta m_{31}^2 < 0$  the combination of both data sets results in an improvement since the local degenerate minimum for data set II lies at a different point in the parameter plane than the one for data set I.

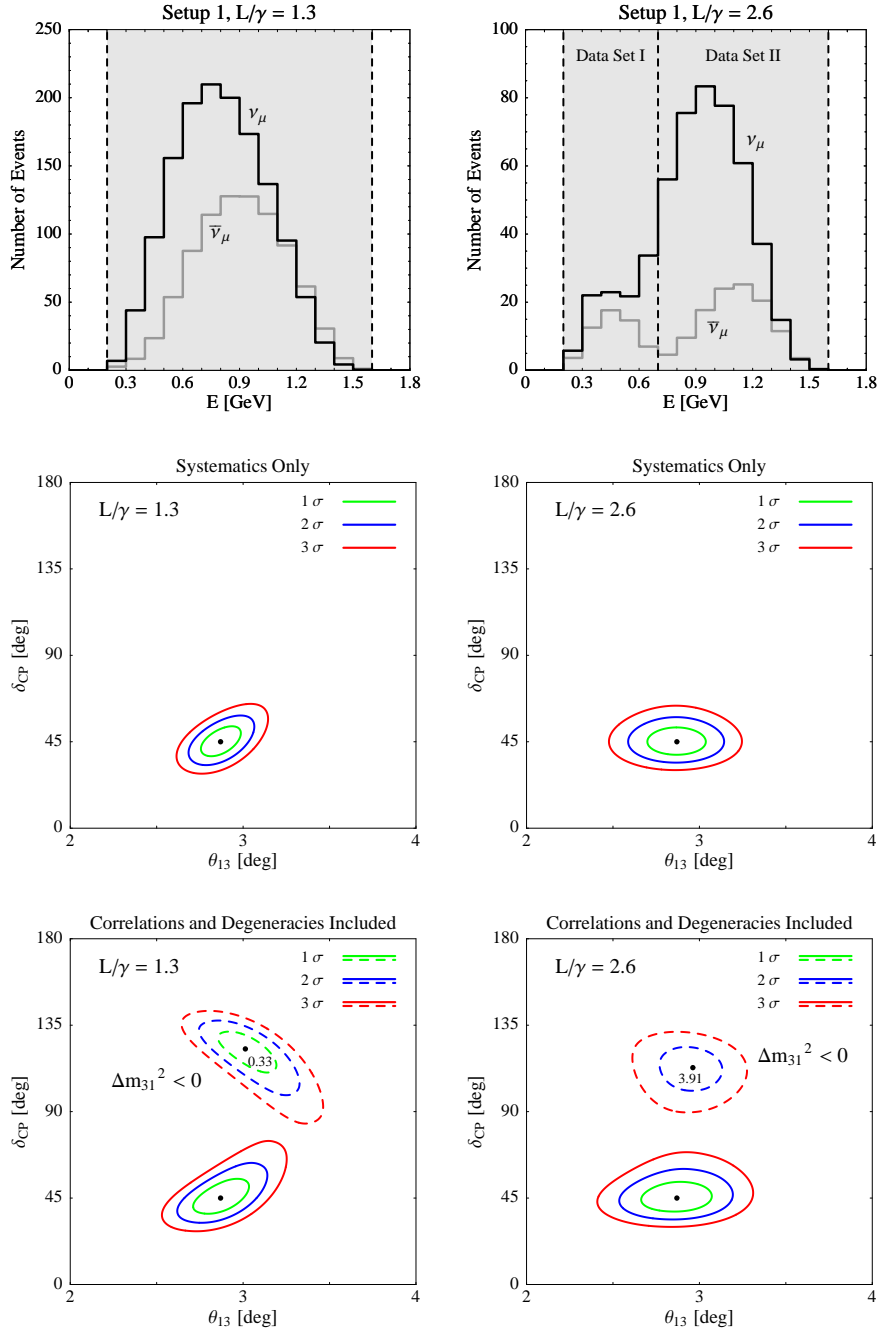


**Figure 15:** Comparison of the performance of Setup 1 at  $L/\gamma=1.3$  (left column) and  $L/\gamma=2.6$  (right column). The oscillation parameters used as input are  $\sin^2 2\theta_{13} = 10^{-2}$ ,  $\delta = \pi/4$  and the other parameters are the ones from Eq. (1). The first row shows the appearance spectra for neutrinos and anti-neutrinos in the energy window of the analysis (gray area). The second row shows the allowed regions in the  $\theta_{13}$ - $\delta$  plane at 1, 2, and 3  $\sigma$  with only taking systematics into account, while in the third row also correlations and degeneracies are included. The value next to the local minimum in the degenerate solution (fitted with  $\Delta m_{31}^2 < 0$ ) indicates the value of  $\Delta\chi^2$  at the local minimum.

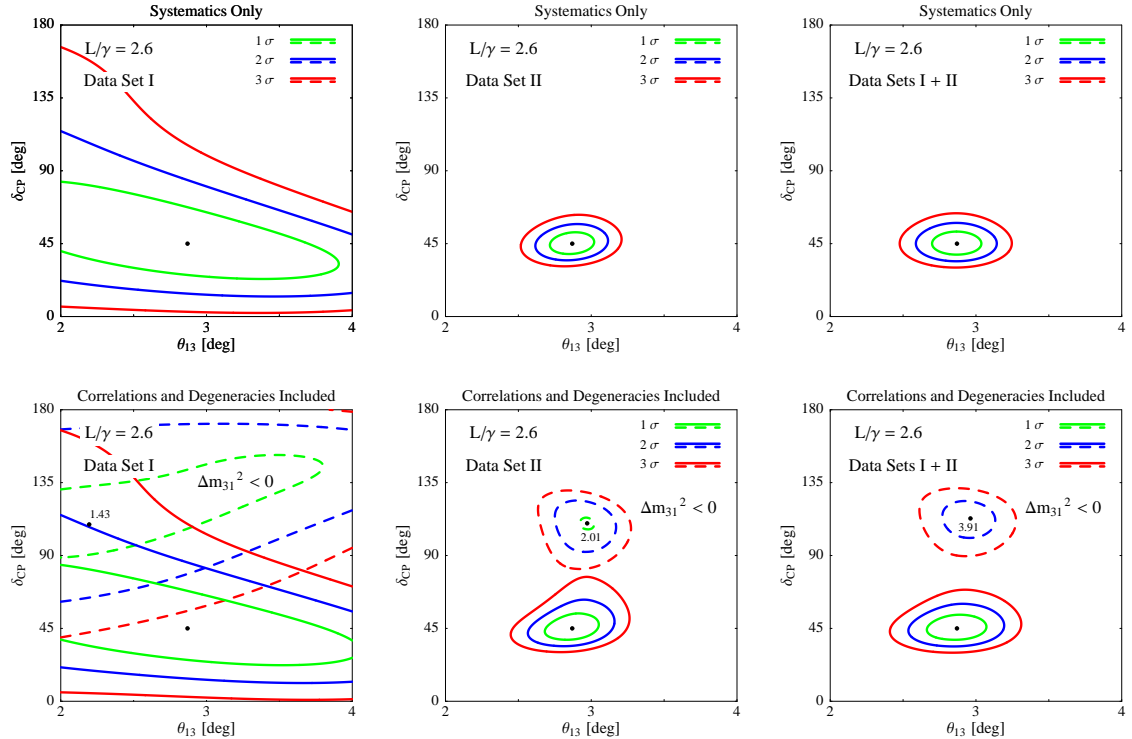


**Figure 16:** The allowed regions in the  $\theta_{13}$ - $\delta$  plane at 1, 2, and 3  $\sigma$  for Setup-I with  $L/\gamma=2.6$ . In the upper row only systematics are taken into account while in the lower row also correlations and degeneracies are included. The allowed regions are shown for the separated data sets I (first column) and II (second column) as explained in the text (see also Fig. 15). In the third column the allowed regions for the combination of both data sets is shown. The value next to the local minimum in the degenerate solution (fitted with  $\Delta m_{31}^2 < 0$ ) indicates the value of  $\Delta\chi^2$  at the local minimum.

## References

- [1] Y. Itow *et al.*, KEK report 2001-4, [hep-ex/0106019](#).
- [2] D. S. Ayres *et al.* (NOvA) (2004), [hep-ex/0503053](#).
- [3] K. Nakamura, Int. J. Mod. Phys. **A18**, 4053 (2003).
- [4] C. Albright *et al.* [hep-ex/0008064](#), and references therein.
- [5] A. Blondel *et al.*, Nucl. Instrum. Meth. **A451**, 102 (2000).
- [6] M. Apollonio *et al.* (2002), [hep-ph/0210192](#).
- [7] P. Zucchelli, Phys. Lett. **B532**, 166 (2002).
- [8] J. Bouchez, M. Lindroos, and M. Mezzetto, AIP Conf. Proc. **721**, 37 (2004), [hep-ex/0310059](#).
- [9] M. Mezzetto, J. Phys. **G29**, 1771 (2003), [hep-ex/0302007](#).
- [10] J. Burguet-Castell, D. Casper, J. J. Gomez-Cadenas, P. Hernandez, and F. Sanchez, Nucl. Phys. **B695**, 217 (2004), [hep-ph/0312068](#).
- [11] F. Terranova, A. Marotta, P. Migliozzi, and M. Spinetti, Eur. Phys. J. **C38**, 69 (2004), [hep-ph/0405081](#).
- [12] A. Donini, E. Fernandez-Martinez, P. Migliozzi, S. Rigolin, and L. Scotto Lavina (2004), [hep-ph/0406132](#).
- [13] M. Mezzetto, Nucl. Phys. Proc. Suppl. **143**, 309 (2005), [hep-ex/0410083](#).
- [14] C. Albright *et al.* (Neutrino Factory/Muon Collider) (2004), [physics/0411123](#).
- [15] A. Donini, E. Fernandez-Martinez, and S. Rigolin (2004), [hep-ph/0411402](#).
- [16] J. Burguet-Castell, D. Casper, E. Couce, J. J. Gomez-Cadenas, and P. Hernandez (2005), [hep-ph/0503021](#).
- [17] S. K. Agarwalla, A. Raychaudhuri, and A. Samanta (2005), [hep-ph/0505015](#).
- [18] A. Donini, D. Meloni, and S. Rigolin (2005), [hep-ph/0506100](#).
- [19] A. Cervera *et al.*, Nucl. Phys. **B579**, 17 (2000), [hep-ph/0002108](#).
- [20] M. Freund, P. Huber, and M. Lindner, Nucl. Phys. **B585**, 105 (2000), [hep-ph/0004085](#).
- [21] C. Volpe, J. Phys. **G30**, L1 (2004), [hep-ph/0303222](#).
- [22] J. Serreau and C. Volpe, Phys. Rev. **C70**, 055502 (2004), [hep-ph/0403293](#).

- [23] P. Huber, M. Lindner, and W. Winter, Comput. Phys. Commun. **167**, 195 (2005), <http://www.ph.tum.de/~globes>, hep-ph/0407333.
- [24] G. L. Fogli, E. Lisi, A. Marrone, and D. Montanino, Phys. Rev. **D67**, 093006 (2003), hep-ph/0303064.
- [25] J. N. Bahcall, M. C. Gonzalez-Garcia, and C. Pena-Garay, JHEP **08**, 016 (2004), hep-ph/0406294.
- [26] A. Bandyopadhyay, S. Choubey, S. Goswami, S. T. Petcov, and D. P. Roy (2004), hep-ph/0406328.
- [27] M. Maltoni, T. Schwetz, M. A. Tortola, and J. W. F. Valle, New J. Phys. **6**, 122 (2004), hep-ph/0405172.
- [28] M. Apollonio *et al.* (CHOOZ), Phys. Lett. **B466**, 415 (1999), hep-ex/9907037.
- [29] P. Huber, M. Lindner, and W. Winter, Nucl. Phys. **B645**, 3 (2002), hep-ph/0204352.
- [30] P. Huber, M. Lindner, and W. Winter, Nucl. Phys. **B654**, 3 (2003), hep-ph/0211300.
- [31] R. J. Geller and T. Hara, Phys. Rev. Lett. **49**, 98 (2001), hep-ph/0111342.
- [32] T. Ohlsson and W. Winter, Phys. Rev. **D68**, 073007 (2003), hep-ph/0307178.
- [33] S. V. Panasyuk, *Rem (reference earth model) web page* (2000), <http://cfauc5.harvard.edu/lana/rem/index.htm>.
- [34] B. Autin *et al.*, J. Phys. **G29**, 1785 (2003), physics/0306106.
- [35] A. Ereditato and A. Rubbia, Nucl. Phys. Proc. Suppl. **139**, 301 (2005), hep-ph/0409143.
- [36] M. Mezzetto, private communications.
- [37] M. Mezzetto (2005), talk given at NNN 2005, Aussois, France, [nnn05.in2p3.fr/trans/mezzetto.pdf](http://nnn05.in2p3.fr/trans/mezzetto.pdf).
- [38] J. J. Gomez-Cadenas *et al.* (CERN working group on Super Beams) hep-ph/0105297.
- [39] Y. Kozlov, L. Mikaelyan, and V. Sinev, Phys. Atom. Nucl. **66**, 469 (2003), hep-ph/0109277.
- [40] H. Minakata, H. Sugiyama, O. Yasuda, K. Inoue, and F. Suekane, Phys. Rev. **D68**, 033017 (2003), hep-ph/0211111.
- [41] P. Huber, M. Lindner, T. Schwetz, and W. Winter, Nucl. Phys. **B665**, 487 (2003), hep-ph/0303232.
- [42] P. Litchfield and L. Mualem, *Results of simulations of the Liquid scintillator detector*, Tech. Rep. Nova-NOTE-SIM-42, NOvA (2004).

- [43] P. Litchfield and L. Mualem, *Comparison of the energy resolution of the standard and totally active scintillator detectors*, Tech. Rep. Nova-NOTE-SIM-48, NOvA (2004).
- [44] P. Litchfield, private communication.
- [45] C. K. Jung (1999), [hep-ex/0005046](#).
- [46] P. Huber, M. Lindner, M. Rolinec, T. Schwetz, and W. Winter, Phys. Rev. **D70**, 073014 (2004), [hep-ph/0403068](#).
- [47] J. Burguet-Castell, M. B. Gavela, J. J. Gomez-Cadenas, P. Hernandez, and O. Mena, Nucl. Phys. **B608**, 301 (2001), [hep-ph/0103258](#).
- [48] H. Minakata and H. Nunokawa, JHEP **10**, 001 (2001), [hep-ph/0108085](#).
- [49] M. Lindroos (2005), talk given at the joint ECFA/BENE meeting, March 16, 2005, CERN, <http://nuspp.in2p3.fr/Bene/BENEWeekMarch05/>.
- [50] P. Huber and W. Winter, Phys. Rev. **D68**, 037301 (2003), [hep-ph/0301257](#).
- [51] V. Barger, D. Marfatia, and K. Whisnant, Phys. Rev. **D65**, 073023 (2002), [hep-ph/0112119](#).
- [52] M. Diwan *et al.* (2002), [hep-ex/0211001](#).
- [53] P. Huber, M. Lindner, and W. Winter (2004), [hep-ph/0412199](#).
- [54] W. Winter, Phys. Lett. **B613**, 67 (2005), [hep-ph/0411309](#).
- [55] A. de Gouvea, J. Jenkins, and B. Kayser (2005), [hep-ph/0503079](#).